Journal of the American Heart Association

ORIGINAL RESEARCH

Panoramic Endocardial Optical Mapping Demonstrates Serial Rotors Acceleration and Increasing Complexity of Activity During Onset of Cholinergic Atrial Fibrillation

Óscar Salvador-Montañés (iD), MD; Rafael J. Ramirez (iD), PhD; Yoshio Takemoto (iD), MD, PhD; Steven R. Ennis, PhD; Daniel Garcia-Iglesias, MD, PhD; Sicong Wang, MSc; Patrick J. Wolfer, BSc; Jiang Jiang, BSc; Sergey V. Mironov, PhD; Sandeep V. Pandit, PhD; José Jalife (iD), MD, PhD; Omer Berenfeld (iD), PhD

BACKGROUND: Activation during onset of atrial fibrillation is poorly understood. We aimed at developing a panoramic optical mapping system for the atria and test the hypothesis that sequential rotors underlie acceleration of atrial fibrillation during onset.

METHODS AND RESULTS: Five sheep hearts were Langendorff perfused in the presence of 0.25 µmol/L carbachol. Novel optical system recorded activations simultaneously from the entire left and right atrial endocardial surfaces. Twenty sustained (>40 s) atrial fibrillation episodes were induced by a train and premature stimuli protocol. Movies obtained immediately (Initiation stage) and 30 s (Early Stabilization stage) after premature stimulus were analyzed. Serial rotor formation was observed in all sustained inductions and none in nonsustained inductions. In sustained episodes maximal dominant frequency increased from (mean±SD) 11.5±1.74 Hz during Initiation to 14.79±1.30 Hz at Early Stabilization ($P<0.0001$) and stabilized thereafter. At rotor sites, mean cycle length (CL) during 10 prerotor activations increased every cycle by 0.53% ($P=0.0303$) during Initiation and 0.34% ($P=0.0003$) during Early Stabilization. In contrast, CLs at rotor sites showed abrupt decreases after the rotors appearances by a mean of 9.65% ($P<0.0001$) during both stages. At Initiation, atria-wide accelerations and decelerations during rotors showed a net acceleration result whereby post-rotors atria-wide minimal CL (CLmin) were 95.5±6.8% of the prerotor CLmin ($P=0.0042$). In contrast, during Early Stabilization, there was no net acceleration in CLmin during accelerating rotors (prerotor=84.9±11.0% versus postrotor=85.8±10.8% of Initiation, $P=0.4029$). Levels of rotor drift distance and velocity correlated with atria-wide acceleration. Nonrotor phase singularity points did not accelerate atria-wide activation but multiplied during Initiation until Early Stabilization. Increasing number of singularity points, indicating increased complexity, correlated with atria-wide CLmin reduction ($P<0.0001$).

CONCLUSIONS: Novel panoramic optical mapping of the atria demonstrates shortening CL at rotor sites during cholinergic atrial fibrillation onset. Atrial fibrillation acceleration toward Early Stabilization correlates with the net result of atria-wide accelerations during drifting rotors activity.

Key Words: atrial fibrillation ■ dominant frequency ■ optical mapping ■ rotors ■ singularity points

CLINICAL PERSPECTIVE

What Is New?

- We developed a new panoramic endoscopic system enabling optical mapping of activation patterns simultaneously across intact endocardial surfaces of right and left atria in the isolated sheep heart to study how initial triggered activity turns into subsequent high frequency and complex excitation waves in a self-sustained cholinergic atrial fibrillation model.
- Ectopies or wavebreaks following a premature stimulus can occur in the other atrium and subsequent fibrillation is sustained only when the cycle intervals gradually shorten and rotors appear.
- Rotors appear serially and temporarily accelerate activation in their vicinity, but the rotors' acceleration is associated with net atria-wide acceleration only initially and is followed by an equilibration between atria-wide accelerations and decelerations; wavebreaks that do not develop into reentries do not associate with atrial acceleration at any stage, but their number, and hence fibrillation complexity, is increasing with time until stabilization.

What Are the Clinical Implications?

- The appearance of initial ectopic waves, wavebreaks, and rotor patterns across the 2 atria during the onset of atrial fibrillation is consistent with the suggestion that discharges and driving activity can appear across the entire atria and in locations remote to the triggering event, which warrant panoramic mapping.
- Only a subset of drifting rotors patterns associate with atria-wide acceleration, sustenance and increased complexity, and specifically targeting those patterns could potentially improve ablative and nonablative therapies.

Nonstandard Abbreviations and Acronyms

APD	action potential duration
BT	breakthrough pattern of impulse propagation
CL	cycle length
CLmin	5% minimal CL
DF	dominant frequency
DFmax	maximal DF
SP	phase singularity point

Atrial fibrillation (AF), the most common sustained clinical arrhythmia, is a challenging disease.[1] It would be advantageous to better understand the initiation of AF to avoid its stabilization and prevent its progression. It is commonly accepted that triggered activity in patients can initiate AF episodes and indeed, AF episodes often follow the appearance of spontaneous repetitive focal activity of variable origin.[2,3] However the manner by which the discrete initial triggered activity turns into subsequent high frequency and complex excitation waves and self-sustained AF remains elusive.[3,4]

Optical mapping of the posterior left atrium (LA) in a sheep model of cholinergic AF initiation revealed that programmed pacing at the pulmonary veins generated the first wavebreaks and self-sustained reentries at the septopulmonary bundle.[5] There is also evidence from panoramic electrical mapping in humans that spontaneous or induced AF was initiated in the presence of repetitive focal, but mostly reentrant, patterns.[6] Nevertheless, the dynamics and the role of observed reentrant activity across the 2 atria during initiation and early stabilization of AF have not been fully established. In particular, the mechanisms giving rise to the dramatic increase in activation rate and complexity across the entire atria, characteristic of the transition from organized rhythm to disorganized fibrillation, have not been studied.

Thus, this study has 2 objectives. We first aim at developing a wide-view optical mapping approach to elucidate with high reliability the patterns of excitation across the entire and intact endocardial surfaces of the right atrium (RA) and LA. And second, we aim to use the new panoramic mapping capabilities to test the hypothesis that during the onset of cholinergic AF reentrant activity accelerates with an increased complexity of the fibrillation. Using the panoramic endocardial optical mapping system in isolated sheep hearts we find reentrant-associated acceleration of activity across both the RA and LA. Our results support the notion that series of reentrant activity patterns, but not wavebreaks, underlie the acceleration of AF during onset.

METHODS

This research was performed in its entirely at the University of Michigan in accordance with its Unit of Laboratory Animal Medicine Policies, Guidelines and Standard Operating Procedures. The study data, methods, and materials information will be made available to other researchers for purposes of reproducing the results or procedures upon a reasonable request.

Langendorff Perfused Heart Preparations

Five healthy male sheep weighing 30 to 40 kg were used. The animal protocol was approved by the University Committee on Use and Care of Animals

of the University of Michigan and conforms to the Guide for Care and Use of Laboratory Animals by the US National Institutes of Health. Sheep hearts were isolated and Langendorff perfused as described previously.[7–9] See Data S1 for more details.

AF Induction and Classification

All episodes of atrial activity were studied in the presence of 0.25 µmol/L carbachol mimicking increased vagal tone inducive of AF.[10,11] AF was induced with a stimuli train (S1) and premature stimulus (S2) programmed pacing protocol at the LA epicardial free wall (see Data S1 for details). Subsequent episodes were classified as nonsustained if lasting <40 s and self-sustained if lasting ≥40 s.[12] All nonsustained and all sustained AF episodes were included in the analysis. We focused on 2 periods of the AF onset: the first 7 s post-S2 period (termed Initiation period), and 30 to 40 s post-S2 (termed Early Stabilization period).

Wide-View Endoscopic Optical Mapping

The novel wide-view, panoramic, endoscopic mapping approach is described in Data S1 and Figure S1. Briefly, lesions were cut at left and right ventricular apexes to enable insertion of 2 dual-channel solid borescopes equipped with wide-view objective units directed toward the left and right atria. The borescopes were attached to cameras to record di-4-ANEPPS fluorescence from the endocardial surfaces in 2 10-s duration movies (80 × 80 pixels, 600 frames/s) during the pacing and Initiation and during the Early Stabilization periods. Sample recordings are provided as Supplemental Videos.

Optical Data Analysis

Parameters analyzed in space and time included phases and phase singularity points (SPs), dominant frequencies (DFs), cycle lengths (CLs) and action potential durations (APDs). Details of data processing and definitions of SPs of rotors and non-rotors (wavebreaks), maximal DF (DFmax), atria-wide minimal CL (CLmin) as well as rotors drift distance and velocity are presented as Data S1.

Statistical Analysis

Analyzed values are presented as mean±SD, and with 95% CIs where noted. For time course of measures, repeated values in time were analyzed with linear regressions and ANOVA. Distributions of data values within groups were tested for normality using the Shapiro–Wilk test before all comparisons. For comparisons between normally distributed groups of data, paired or unpaired Student's t test methods were used as appropriate. Unpaired t tests were applied under nonequal variances condition. The nonnormal distributions were compared with Wilcoxon signed-rank test as noted. Statistical analyses were performed in Matlab (MathWorks, Natick, MA). Probability (P) value was considered significant if less than alpha=0.05, except when adjusted for multiple comparisons as noted.

RESULTS

Time Course of AF Onset and Activation Patterns

In 5 hearts, 16 nonsustained AF episodes and 20 induced ≥40 s long AF episodes were analyzed. A representative time course of pacing induction, Initiation, and Early Stabilization of sustained AF is shown in Figure 1. A demonstrates a single pixel optical signal showing transition from a stimuli train S1 and premature stimulus S2 to self-sustained more complex AF activity. During LA pacing the electrical activity was devoid of wavebreaks across either atrium, and APD_{70} for all RA regions was longer than the for all LA regions (112.6±19.3 ms versus 93.9±9.9 ms respectively, $P<0.0001$; see Video S1 and Figure S2). In episodes of self-sustained AF the stimuli train-S2 interval was longer than in nonsustained AF (127±18 ms, n=20, versus 109±15 ms, n=15, respectively; $P=0.017$). B and C demonstrate the increased complexity from the Initiation period, immediately following the S2 stimulus, to the Early Stabilization period 30 s later (see Videos S2 and S4 for Initiation and Videos S3 and S5 for Early Stabilization). The sample phase snapshots in panels B and C show an increase in the number of SPs and the time-space plots show the temporal proliferation of patterns characteristic of reentrant activity, from a single site in the RA (cyan arrow, B) to multiple sites in both atria (C).

Among the 20 sustained AF inductions, the first observed post-S2 waves were 16 breakthrough (BT) and 4 rotor patterns (see Data S1 and Figure S3); the initial BTs appeared in sequences characterized by gradual decrease in activation intervals; rotors were observed in each of the 20 inductions leading to sustained AF (see Figure S4), but none in the inductions that failed to result in sustained AF (see Figure S5). During Initiation there was a trend for rotors to be more abundant in the RA (55.8±18.9%) than in the LA (44.2±18.9%, $P=0.0621$; see Figure S6). Thereafter the transition to Early Stabilization was characterized by a decrease in the RA free wall (from 35.5±18.7% to 25.6±16%, $P=0.0121$) and an increase in the LA roof (from 5.7±6.1% to 10.7±10.5%, $P=0.0187$) rotors presence and a trend to LA dominance over the RA (55.7±23.9% versus 44.3±23.9%, $P=0.0670$).
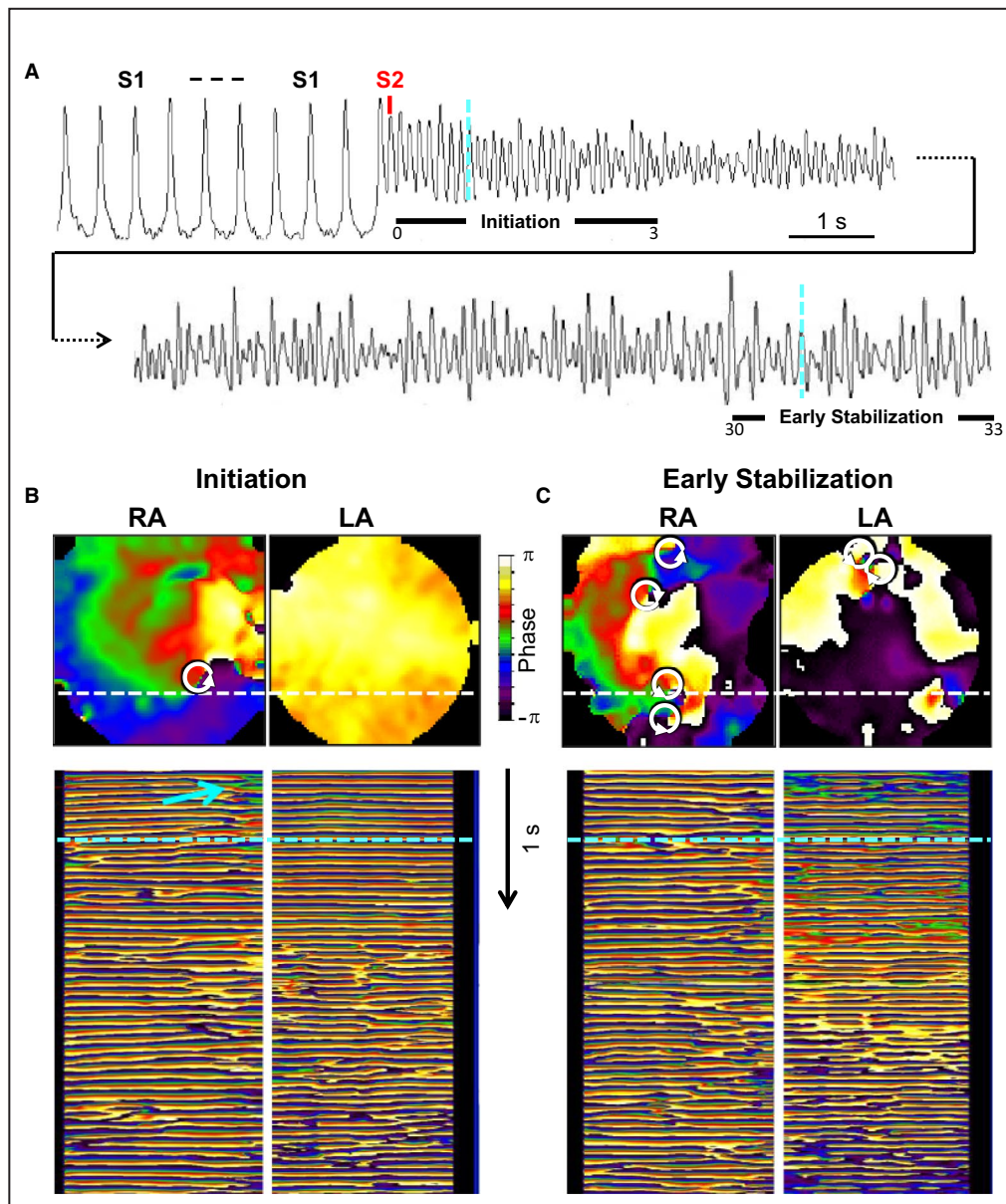
Figure 1. Induction and stages of AF onset.
A, A sample pixel fluorescence trace showing the stage of regular pacing (S1…S1) followed by a premature stimulus (S2) inducing self-sustained AF. The AF onset was analyzed during its Initiation (0–3 s) and Early Stabilization (30–33 s) stages. Cyan vertical dash lines indicate times of phase maps in (**B**) and (**C**). **B**, Phase maps (top) and time-space plots (bottom; along the white dash line in phase maps) during Initiation stage. Arrowhead circle in phase map points to the first rotor activity in the AF (Cyan arrow in the time-space plot). **C**, Phase maps (top) and time-space plots (bottom; along the white dash line in phase maps) during Early Stabilization stage. Arrowhead circles in phase map point to the multiple rotor or wavebreak activity. AF indicates atrial fibrillation; LA, left atrium; RA, right atrium; S1, stimuli train; and S2, premature stimulus.

Acceleration of AF

Acceleration of activation rate during onset of sustained AF episodes was quantified by generating DF maps in 3-s segments during the Initiation stage immediately after induction and during the Early Stabilization stage, 30 s later. Figure 2A shows representative DF maps from a sample heart in the course of AF onset. In this example, the DF map immediately following induction (0–3 s) shows a maximal DF (DFmax) domain of 9 Hz in the RA and most of the remaining atria activate at a DF of 8 Hz. Subsequent DF maps show an increase in DFmax to 11.5 Hz (4–7 s) and to 14 Hz (30–33 s) with reduced domain sizes indicating increased complexity
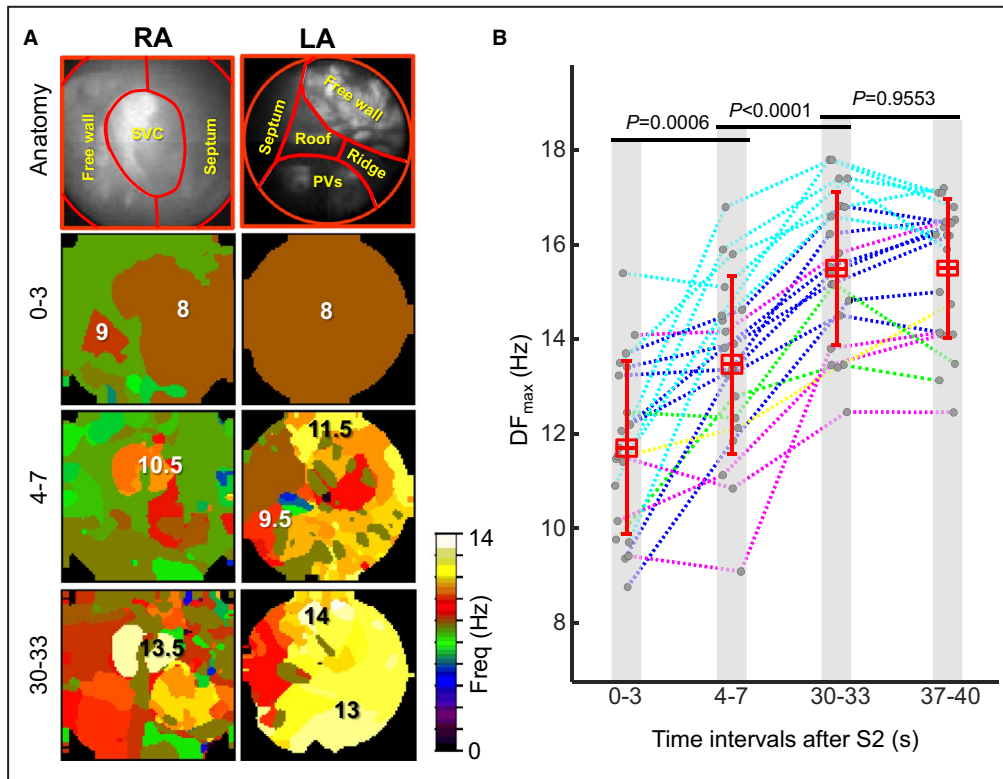
**Figure 2.** Time course of dominant frequencies (DFs) during AF onset.
A, Anatomy image and DF maps in a sample AF induction panoramic mapping of the RA and LA endocardial surfaces. From top to bottom panels: (1) The anatomy image of the panoramically mapped RA and LA. (2) DF maps in the respective atrium and at the indicated time periods (in s). Numbers in panels are sample DF values in Hz. Maximal DF (DFmax) site is seen to shift from the RA at 0 to 3 s to the LA afterwards. **B**, DFmax progression over time in all inductions (N=5 hearts, n=20 inductions). Colors indicate inductions in different hearts (1, 2, 4, 6, and 7 inductions/heart; Shapiro–Wilk test P=0.8584). Red markers indicate mean (horizontal bar), 95% CI of the mean (box) and SD (error bars) values. t test was performed in all the comparisons, except 30 to 33 versus 37 to 40 s, which was compared with Wilcoxon signed-rank test. AF indicates atrial fibrillation; LA, left atrium; PVs, pulmonary veins; RA, right atrium; and SVC, superior vena cava.

of activity.[13] Time course of DFmax values in 20 sustained AF inductions (Figure 2B) demonstrated a progressive averaged increase from an initial value of 11.71±1.82 Hz at 0 to 3 s to 13.45±1.88 Hz at 4 to 7 s (P=0.0006) and to 15.49±1.62 Hz at 30 to 33 s (P<0.0001) after induction. Thereafter, at 37 to 40 s post induction the DFmax values stabilized at 15.48±1.46 Hz (P=0.9553).

Tracking the distribution of DFmax in the various RA and LA regions during the 20 AF inductions reveals that on average the posterior LA is hosting the atrial DFmax during all 4 periods of time analyzed, albeit not always significantly higher than the other regions (Figure S7). Interestingly, despite the posterior LA presenting the highest average DFmax in each period of time, in some inductions, other LA regions as the ridge, the free wall, and the roof presented similar or higher DFmax values. The LA highest DFmax values is also consistent with the lowest paced APD_{70} there (Figure S2) and with previous studies.[14]

Local Acceleration at Rotors Sites

Analysis of time course of CLs in Figure S8 demonstrated gradual AF acceleration and stabilization consistent with DFmax time course in Figure 2. Thus we investigated the relationship between appearance of rotors and acceleration of the AF activation rate, as indicated by the decrease of CLmin anywhere in the atria during AF Initiation. Figure 3A shows representative phase snapshots before, during, and after the appearance of a rotor along with single pixel recordings. The phase maps show the appearance of a SP at time zero. The SP meanders and drifts for some time, as shown at 208 ms, until its disappearance shortly afterwards, before the time of the 438 ms map. Representative single-pixel fluorescence recordings from 2 different locations near the meandering SP (sites a and b in inserts) show sequential CLs with a beat-by-beat variability. To characterize the time-course variation in local CL relative to rotor appearance, the traces in Figure 3A
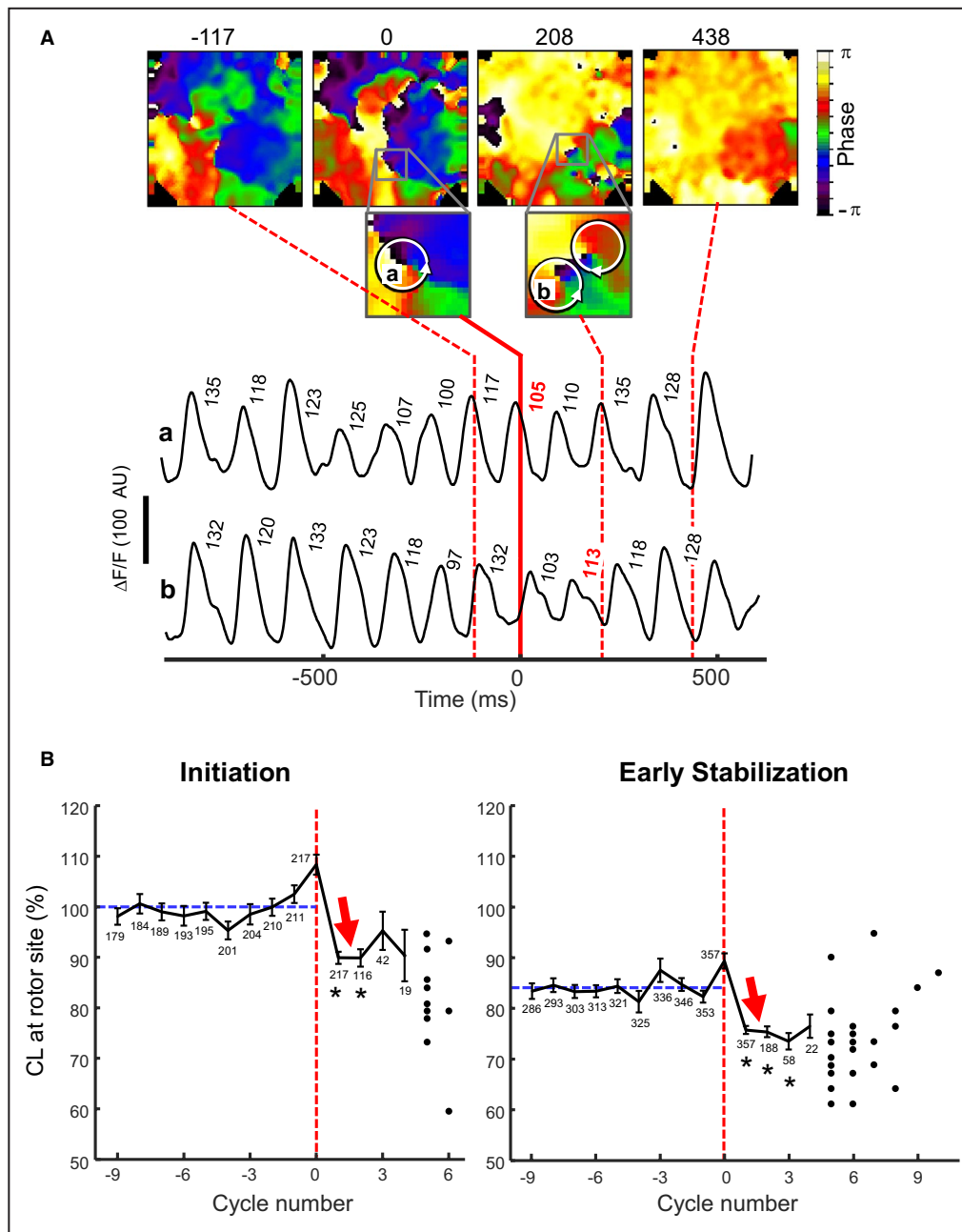
Figure 3.   Time -course of cycle length (CL) of rotors.

A, Representative example of CLs localized to a rotor site. Top: Phase maps showing a prerotor, rotor appearance, rotor drift, and postrotor snapshots at −117, 0, 208, and 438 ms (respectively; time is relative to the moment of rotor appearance). Inserts are magnifications of areas with rotors indicated by the arrowhead circles. Bottom: Sample fluorescence signals from 2 different pixels marked **a** and **b** near the SPs of the meandering rotor in the inserts. Numbers are beat-by-beat CLs in ms. Red numbers indicate the CLs of the rotor in the first (top trace) and second (bottom trace) in ms. Vertical red lines indicate the time of the phase snapshots. **B**, Time course of CLs of activity at the rotors sites during the Initiation (left, and Early Stabilization [right] stages of the AF onset [N=5, n=20 in each graph]). X axis is the cycle number of the activity relative to the moment of individual rotors' appearances (cycle number=0; vertical red line). All CL values are presented as percentage of the prerotors averaged CLs (blue horizontal lines) at Initiation. Prerotor CLs were determined at the site of the rotor SP's appearance. Thereafter the CLs were determined at different sites tracking the meandering SPs. Numbers indicate the numbers of CLs analyzed and shown as mean and SD. Dots represent rotors too infrequent for statistical comparisons. Red arrows: highlighting shortening of CLs following rotor appearance. Wilcoxon signed-rank test was performed for all comparisons. AF indicates atrial fibrillation; and SP, phase singularity point. *$P<10^{-4}$ versus prerotors averaged CLs.

were synchronized with their zero times coinciding with the appearance of the SP (solid red line). The traces demonstrate that the local CL near the SP increases from 105 ms during the first cycle of the rotor (red number, top trace), to 113 ms during the second cycle (red number, bottom trace).

The CLs at rotors sites during cycles before and during the rotors identified in 20 inductions of AF were collected using the tracking method shown in A of Figure 3. A total of 217 and 357 rotors detected during Initialization and Early Stabilization stages, respectively, appeared in series at rates of 2.0±1.37 versus 3.29±2.09 rotors/s during the 2 respective stages (P<0.0001; see Data S1 and Figure S9). Their number decreased with number of cycles lifespan before disappearance, as in previous studies.[14] The rotors completed ≤6 cycles during Initiation and ≤10 cycles during Early Stabilization before dissipating, but the number of their cycles lifespan was not different (1.75±1.03 versus 1.76±1.2 rotations per rotor; P=0.9048).

Figure 3B shows the time course of the normalized local CLs for each cycle during Initiation (left) and Early Stabilization (right) as a function of cycle number, indexed with their zero as the last cycle before the rotor SP appearance. The average collective value of the local CLs in sites of SPs, during 10 cycles before the appearance of the SPs showed a reduction from 108.6±29.2 ms at Initiation to 91.8±31.1 ms at Early Stabilization (15.4% reduction of means, P<0.0001). Regression analyses of cycle-by-cycle 10 prerotor local CLs demonstrated a slow increase: 0.75 ms/cycle (P=0.0014) during Initiation and 0.38 ms/cycle (P=0.0333) during Early Stabilization. In contrast, the local CL following rotor appearance showed an abrupt acceleration with a reduction in the first rotation cycle to 97.7±20.3 ms (9.9%, P<0.0001) during Initiation and to 82.4±16.4 ms (10.2%, P<0.0001) during Early Stabilization. The average local CL of the first 2 cycles of rotors during Initiation (P<0.0001) and 3 cycles of rotors during Early Stabilization (P<0.0001) is 9.65% shorter than that during the past 10 cycles before the appearance of the SP (red arrows in Figure 3B). The local CL of succeeding cycles of the rotors either increased back to the prerotor values, or were too infrequent for statistical comparison.

## Atria-Wide CL Acceleration During Rotors Presence

The changes in CLs across the entire atria and AF onset during the specific times concurrent with the rotors are analyzed in Figure 4. A shows a synchronized sequence of panoramic phase (top) and CL (bottom) snapshots from the LA along with a single pixel recording. The phase maps include SPs at the pivoting center of either rotors or nonrotor (<1 rotation) patterns

of activation. The CL maps show the spatial distribution of the CLs at a particular time and enable determination of minimal CL (CLmin) values across the atria pre- and postrotor presence. In this example, atrial CL before the rotor appearance is 110 ms and it decreases to 70 and 67 ms during the leftward drifting rotor presence. Once the rotor SP disappears a minimal atrial CL of 67 ms is observed.

We collected atria-wide CLmin values immediately before and after multiple SPs in 20 AF inductions to investigate whether SPs of rotor and nonrotor patterns were associated with acceleration of activation rate. Figure 4B shows cumulative analysis of the atrial CLmin values immediately before and after 572 rotor SPs and 661 nonrotor SPs for all inductions (28.6±9.3 and 33±2.6 SPs per induction, respectively). To account for interinduction variability, CLmin data was normalized by the average of the values measured immediately before appearance of rotors and nonrotors SPs during Initiation at each induction separately. During Initiation, the average atrial postrotor CLmin was 95.5±6.8% of the atrial prerotor CLmin (P=0.0042, red arrow) and the atrial nonrotor post-SP was 99.7±1.5% of the atrial pre-SP CLmin (P=0.1737). During transition from Initiation to Early Stabilization, atrial CLmin of both rotor and nonrotor SPs accelerated on average for both rotors (12.4±8.8%, P<0.0001) and nonrotors (15.3±7.2%, P<0.0001; green arrows). However, in contrast with the Initiation, during Early Stabilization there was no reduction in atrial CLmin between the appearance and disappearance of the SPs (rotors: 84.9±11.0% to 85.8±10.8%, P=0.4029; nonrotors: 84.5±7.3% to 84.6±7.4%, P=0.4921, respectively).

Variability in Atria-Wide CL During Rotors Presence

The difference between pre- and postrotors CL values across the atria varied greatly among inductions and stages of AF. Although the example in Figure 4A shows atrial postrotor CL reduction (acceleration), another example shown in Figure S10 is demonstrating an atrial postrotor CL increase (deceleration) during the presence of a rotor that drifts less than the one in Figure 4A. In Figure S11, atria-wide CLmin before specific rotors were compared with CLmin subsequent to the same rotors. Analysis of all prerotor and postrotor atrial CLmin values revealed that 53.8% of rotors during Initiation associated with CLmin reduction and the rest with CLmin increase. The entire group of rotors during Initiation of AF associated with a small but significant atrial CLmin net decrease (acceleration) from 90.2±32.3 to 87.3±33 ms (P=0.0439. See Discussion section). On the other hand, a similar analysis of all prerotor and postrotor atrial CLmin values during
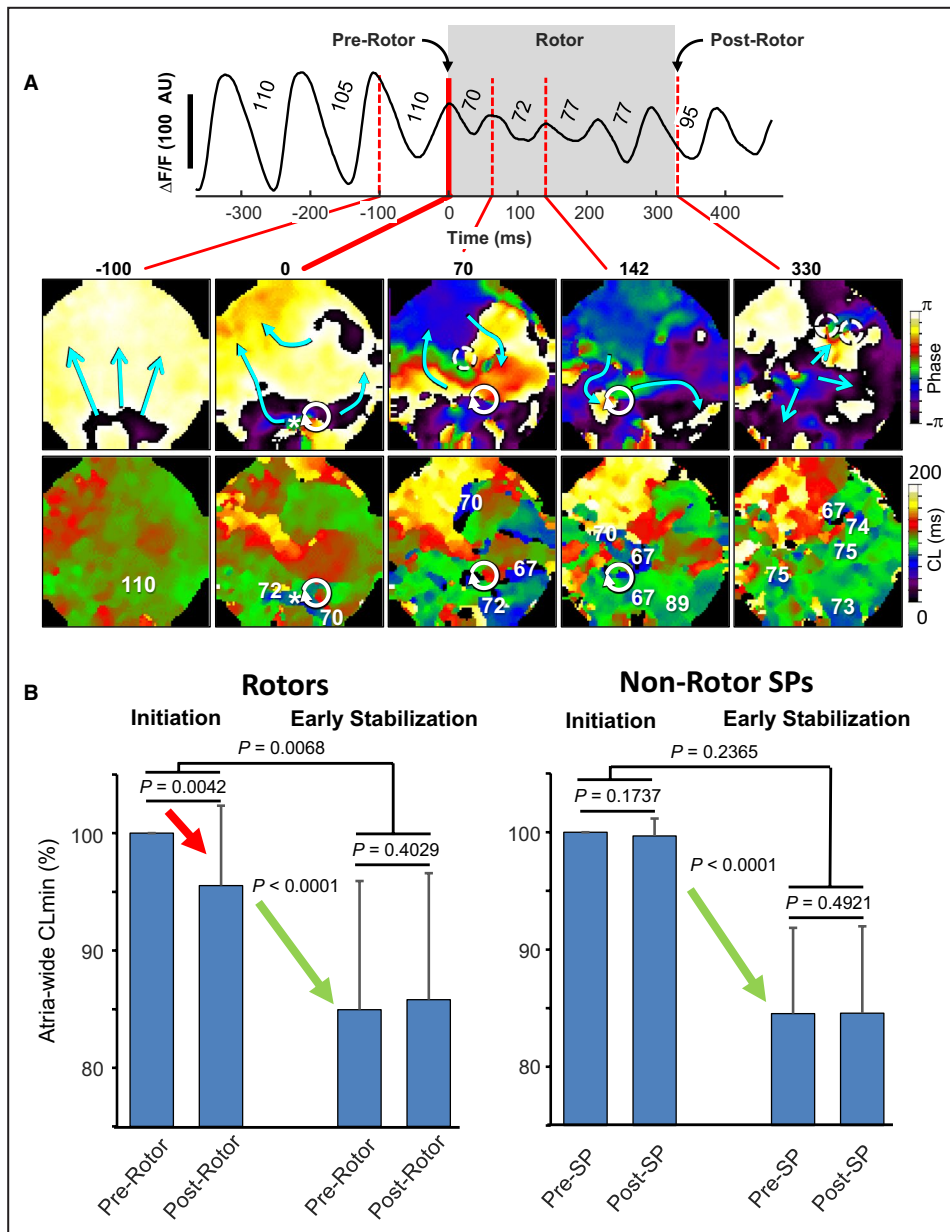
Figure 4. The effect of rotors on the atrial CLs.

A, Fluorescence signal from a sample LA rotor site with corresponding phase (top row) and CL (bottom row) maps. Numbers superimposed on the fluorescence signal and in the CL maps indicate corresponding CLs in ms. Asterisks in CL maps indicate the site of the fluorescence signal near the rotor. The minimal atrial CL is seen in this sample drifting rotor to shorten from a value of 110 ms before the rotor formation to 67 ms it disappears (see CL maps at −100 and 330 ms respectively). Prerotor and postrotor black arrow markers in the fluorescence trace indicate times of determining atria-wide CLmin in analysis. Solid arrowhead circles: location of a sample clockwise rotor in phase maps superimposed in same location also on CL maps. Dashed line circles: locations of sample nonrotor SPs. **B**, Alterations in the atrial CLmin of the AF during the presence of rotors (left bar graph) and nonrotors SPs (<1 rotation; right bar graph). CLmin values were averaged for all pre- and postrotors and nonrotor (SPs) activities in each individual 20 AF inductions in 5 hearts and are presented as mean±SD percentages of the preactivities CLs during the Initiation stage of AF onset of the corresponding induction. Number of rotors: 10.5±3.4 rotors/induction at Initiation and 18.1±6.8 rotors/induction at Early Stabilization. Nonrotors: 15.7±1.9 SPs/induction at Initiation and 17.4±1.2 SPs/induction at Early Stabilization. Red arrow: 4.5±6.8% (P=0.0042) shortening of CLmin of the AF from prerotor to postrotor values during Initiation. Green arrows: Shortening of CLmin of the AF from Initiation to Early Stabilization average values for both rotors (12.4±8.8%, P<0.0001) and non-rotors (15.3±7.2%, P<0.0001) activity. *t* test performed for all comparisons. AF indicates atrial fibrillation; CL, cycle length; CLmin, 5% minimal cycle length; and SP, phase singularity point.

Early Stabilization showed no net difference (prerotor: 77.6±26 versus postrotor: 78.7±26.9 ms, P=0.1671). Overall, the presence of rotors that accelerate locally was distinctively associated with a net atria-wide acceleration of AF at Initiation versus a stable AF rate at Early Stabilization (P=0.0112, see Figure S11). In contrast to the rotors, the nonrotor SPs did not associate with cumulative reduced CLmin either during Initiation or during Early Stabilization (Figure S12).

The Dynamics of Rotors Drift and Atria-Wide CLs

Phase maps in Figure 4A show atria-wide CL acceleration concurrent with a rotor that drifts more than in atria-wide CL deceleration (Figure S10). Thus in Figure 5 we quantify the relationship between rotors drift distance and velocity with the atria-wide CLmin acceleration and deceleration. A shows a general abbreviation of CLs in the LA peripheral sites that are activated by waves emanating from a drifting rotor (see Video S6). The distance and velocity of the rotor drift were measured along a vector connecting the beginning and ending locations of the SP trajectory (see Data S1). The drift data were further correlated with the atria-wide CLmin acceleration or deceleration during the Initiation and Early Stabilization stages in Panel B. The graphs show that when considering all the rotors together, their drift distances decreased from 21.5±15.8 mm at Initiation to 17.9±12.2 mm at Early Stabilization (P=0.0015), but their drift velocities did not alter during that transition and remained at 0.10±0.07 mm/ms; (P=0.4442). Comparing between atria-wide acceleration and deceleration during Initiation revealed a trend for larger distance (23.1±15.7 versus 19.5±15.8 mm, P=0.0523) and significantly larger velocity (0.11±0.07 versus 0.09±0.06 mm/ms, P=0.0103) of drift in rotors with atria-wide acceleration versus deceleration (red arrows). In contrast, during Early Stabilization there were no observed differences in drift distance and velocity in the atria-wide acceleration versus deceleration groups.

Spatial Distribution of Rotors With Atria-Wide Acceleration

In Figure 3 we demonstrate that on average all rotors abbreviate the CL near their core, but Figure 4 and Figure S11 show that only portions of the rotors abbreviate the atrial CLmin and accelerate the AF, thus raising the question of whether only certain regions are dominating the acceleration. In Figure 6 we demonstrate the regional distribution of those rotors that exclusively associate with AF acceleration in the 20 AF inductions. It is shown that all regions harbor such rotors but with varying proportions. On average,

at Initiation the RA tended to have more rotors than in the LA (33.8±17% versus 23±15.2% respectively, P=0.0429) and their numbers became nonsignificantly different at Early Stabilization (22.8±12.8% versus 24±9.7% respectively, P=0.6948). The main regions responsible for the RA-LA equalization in the number of AF acceleration-associated rotors in Early Stabilization were the RA free wall, showing a reduction from 22.4±16.7% to 13.9±10.3% (P=0.0252), and the LA roof, showing an increase from 2.3±3.4% to 5.3±6% (P=0.0084).

Time Course of Complexity During AF Onset

The CL acceleration at the rotors sites and across the atria during arrhythmias onset found in our experiments should be linked to an increase in wave complexity. To demonstrate such conjecture, we counted the number of SPs per frame during 5-s periods of Initiation and Early Stabilization. Figure 7A shows the number of SPs counted in bins of 100 ms during Initiation (left) and Early Stabilization (right) stages of a sample AF induction. In this example, the number of SPs gradually increased during Initiation at an average rate of 3.93e-3 SP/ms (P<0.0001) and then their number stabilized with an average of 17.39 SPs for every 100 ms (P=0.795). In B we summarize the rate of change in SP numbers over 20 AF inductions. On average, during both Initiation and Early Stabilization of AF in our model the number of SPs increases with time, but the rate of increase is reduced from 2.76e-3 SP/ms during Initiation to 1.30e-3 SPs/ms during Early Stabilization (P=0.0056). The complexity of the AF, as quantified by the number of SPs, was further compared to the minimal CL in the atria at the moment SPs were detected throughout Initiation and Early Stabilization. The logarithmic scatter plot in Figure 7C shows the relationship between the number of SPs in 100 ms bins versus the atrial CLmin in that bin for each heart separately. Although each heart shows a different trend, all showed a negative log-log slope, indicating a similar behavior of an increase in the number of SPs for shorter CLs. A linear regression model for log-log data on 1875 SPs and their instantaneous CLs in the 20 inductions in 5 hearts (not shown) had a slope of −4.7667±0.1531 and an intercept of 5.7594±0.0358 (P<0.0001).

DISCUSSION

Main Results

We developed a new panoramic optical method enabling simultaneous mapping of activation patterns across intact atria-wide endocardial surfaces as never before. Using the new system to study the onset of
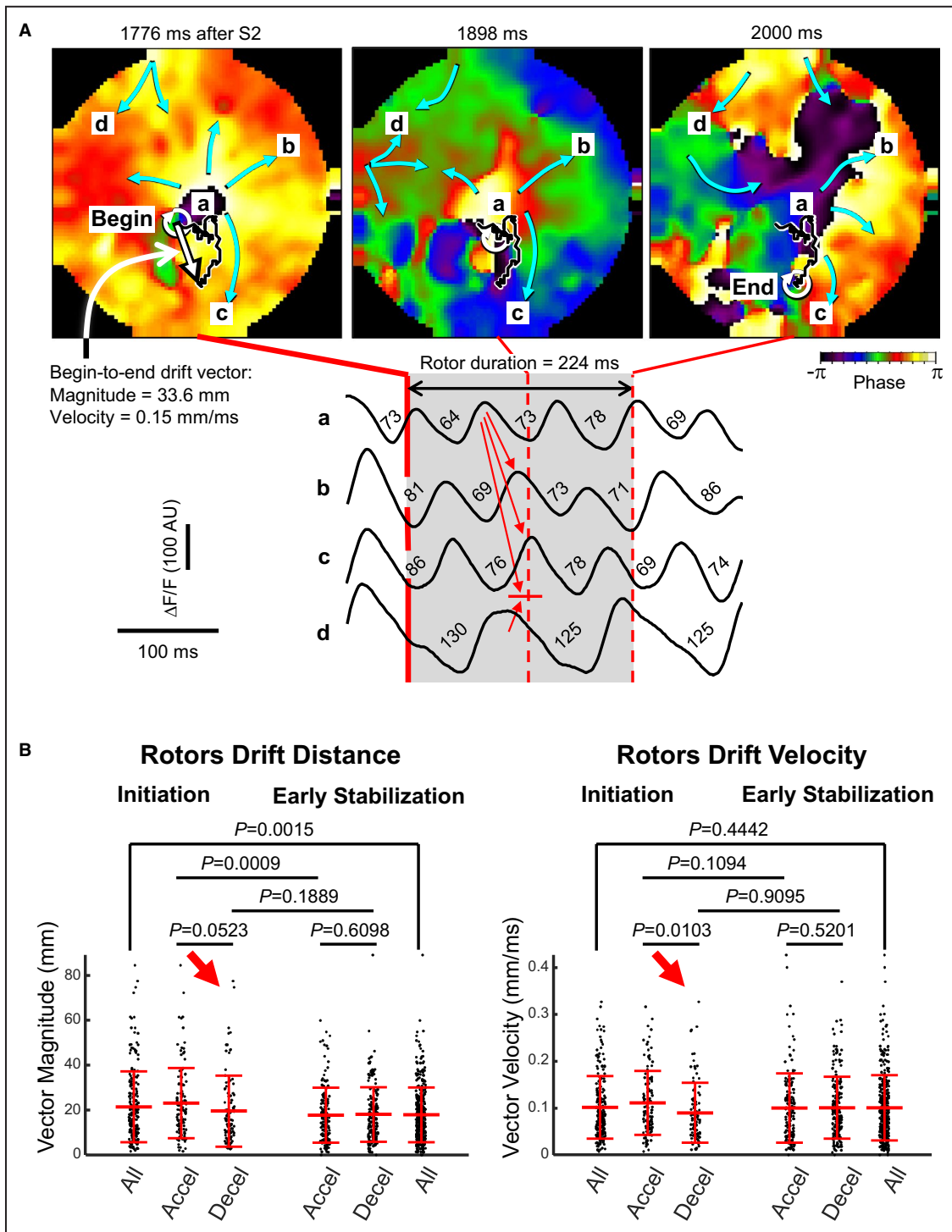
Figure 5. Rotor drift and atria-wide CL alterations.
A, Top: sequential phase maps showing LA activation patterns during the presence of a rotor drifting from start (site begins at 1776 ms after S2) to finish (site ends at 2000 ms; black SP trajectory is superimposed on all maps). Begin-to-end drift vector is shown in leftmost map with distance (vector magnitude) and velocity along the vector (see Data S1). Arrowhead circles indicate location of SP. Bottom: single pixel fluorescence traces from sites near the SP trajectory (**a**) and the periphery (**b–d**) with CLs in ms. CLs in sites **b** and **c** are abbreviated following activating waves emanating from the rotor and SP trajectory area (red arrows). **B**, Left: Rotor drift distance (begin-to-end vector magnitude) for all rotors (All; n=210, n=362), rotors with atria-wide CLmin acceleration (Accel; n=113, n=156) and rotors with atria-wide CLmin deceleration (Decel; n=97, n=206) for Initiation and Early Stabilization (n respectively). Symbols are mean±SD. 95% CI for each distance group is ≤3.1 mm. Right: Rotors drift velocity for same conditions, n numbers and symbols similar as for the left graph. 95% CI for each velocity group is ≤0.0127 mm/ms. Red arrows, indicate trend (left graph) and significant (right graph) decrease differences. CL, cycle length; CLmin, 5% minimal cycle length; LA left atrium; and SP, phase singularity point.

cholinergic AF in the isolated sheep heart, our main observations were that, first, the BTs or wavebreaks following premature stimuli can occur remote from pacing in either atrium, and their succeeding CLs are gradually shortening only when rotors appear and the subsequent AF is sustained. Second, serial short-lasting rotors temporarily accelerate activation in their vicinity, but that acceleration is associated with a net atrial-wide acceleration only during the Initiation stage of the AF and is followed by a net equilibration between acceleration and deceleration maintained during the Early Stabilization stage. Third, distances and velocities of rotors' drifts during atria-wide CL acceleration are greater than during deceleration. And finally, wavebreaks that do not develop into reentries do not associate with net atrial acceleration at any stage, but their number, and hence AF complexity, is increasing with time and atrial acceleration until the Early Stabilization stage.

Wide-View Endoscopic Optical Mapping of AF

The optical signals generated by fluorescence of voltage sensitive dyes in cardiac cells can map their activity with high reliability and spatiotemporal resolution.[15] Although areas covered by optical mapping can typically capture propagation features of fibrillation, they are restricted to visible regions on the atrial epicardium or required a dissection of the atria to map the endocardium,[5] with consequential artificial boundaries and possible ischemia,[16] limiting investigation of epicardial-endocardial activation differences. To avoid the atrial dissection we previously developed an endoscopic approach to map the posterior LA, which is of a major clinical importance.[17,18] As clinical mapping of extracellular potentials have demonstrated possible reentrant and focal drivers of AF distributed over the entire atrial endocardium,[4,6,19,20] it is desirable to use also panoramic optical mapping for a more comprehensive investigation of transmembrane impulse propagation during AF.[21–23] Thus, we developed here a unique objective lens assembly attached via a borescope to a charge-coupled device camera[17] for a panoramic optical mapping of the entire endocardial surfaces viewed above the valves rims of the intact 2 atria. The panoramic view enables tracking the complete trajectory and life span of maximal number of endocardial rotors from their formation to termination.

Activation Patterns and Rotors in AF

Experimental and clinical studies have proposed that rotor activity plays a driving role in the maintenance of AF.[24,25] In a cholinergic and persistent sheep models of AF[8,14,18] rotors have been found to be localized to areas at or adjacent to the highest DF

domains during self-sustained and stable AF, but it is not known what would be the dynamics of those rotors during the onset of AF. Here we tested the hypothesis that the rotors play a role in the acceleration of the activation rate during the transition from the organized and slow rhythm toward the faster and more complex fibrillation. Our panoramic mapping study is demonstrating a dynamic process during AF onset whereby rotors appear serially, are in general short living and discontinuous, and their CLs is shortening by an average of 9.65% in their first 2 to 3 cycles relative to the average CLs before their formation (Figure 3). Despite equal rotor lifespan and local acceleration (Figure 3), the rotors were associated with different atria-wide acceleration dynamics between the Initiation and the Early Stabilization stages of the AF (Figure 4 and Figure S11); greater rotor drift distances and velocities were associated with AF acceleration during Initiation (Figure 5). In contrast, the activity following the formation of SPs that do not complete at least 1 rotation (ie, wavebreaks) did not show a cumulative CLs shortening at any stage of the AF, and their multiplication is suggested to be secondary to the rotor-induced acceleration toward the Early Stabilization of the arrhythmia (Figures 4, 7, and Figure S12).[16]

Our findings are consistent with other studies in patients and simulations showing evidence for rotational activity linked to transient highest activation rate and dominant frequency.[26–28] However our study further finds for the first time that the acceleration at the rotors sites, although brief, associates with the progression of the AF. It was found that following an initial brief breakthroughs period, AF accelerations occurred only when rotors were observed and were otherwise absent during the 10 prerotor cycles (Figure 3B) and during the nonrotors wavebreaks (Figure 4B and Figure S12).

The acceleration of the atria surrounding the accelerating rotors is not universal. Inspection of each rotor separately (Figure S11) finds that in some cases the postrotor activity at surrounding tissue accelerates relative to the prerotor rate, and in other cases the activity decelerates. Data presented in Figure S11 show that each rotor during the Initiation stage reduces the atrial CLmin by a small, but statistically significant, average amount of 90.2 − 87.3=2.9 ms. This small net average acceleration during a rotor presence, if confirmed, may accumulate in time and explain the large atria-wide reduction of CLmin (Figure S8) and increase of DFmax (Figure 2B) during the Initiation stage. The balance between the postrotor accelerating and decelerating atrial activity was found to shift from a small dominating acceleration during Initiation of the AF, to an equilibration during the Early Stabilization stage at about 30 s into the AF. For comparison, in the cases of nonrotors SPs, the atria-wide acceleration is balanced with the
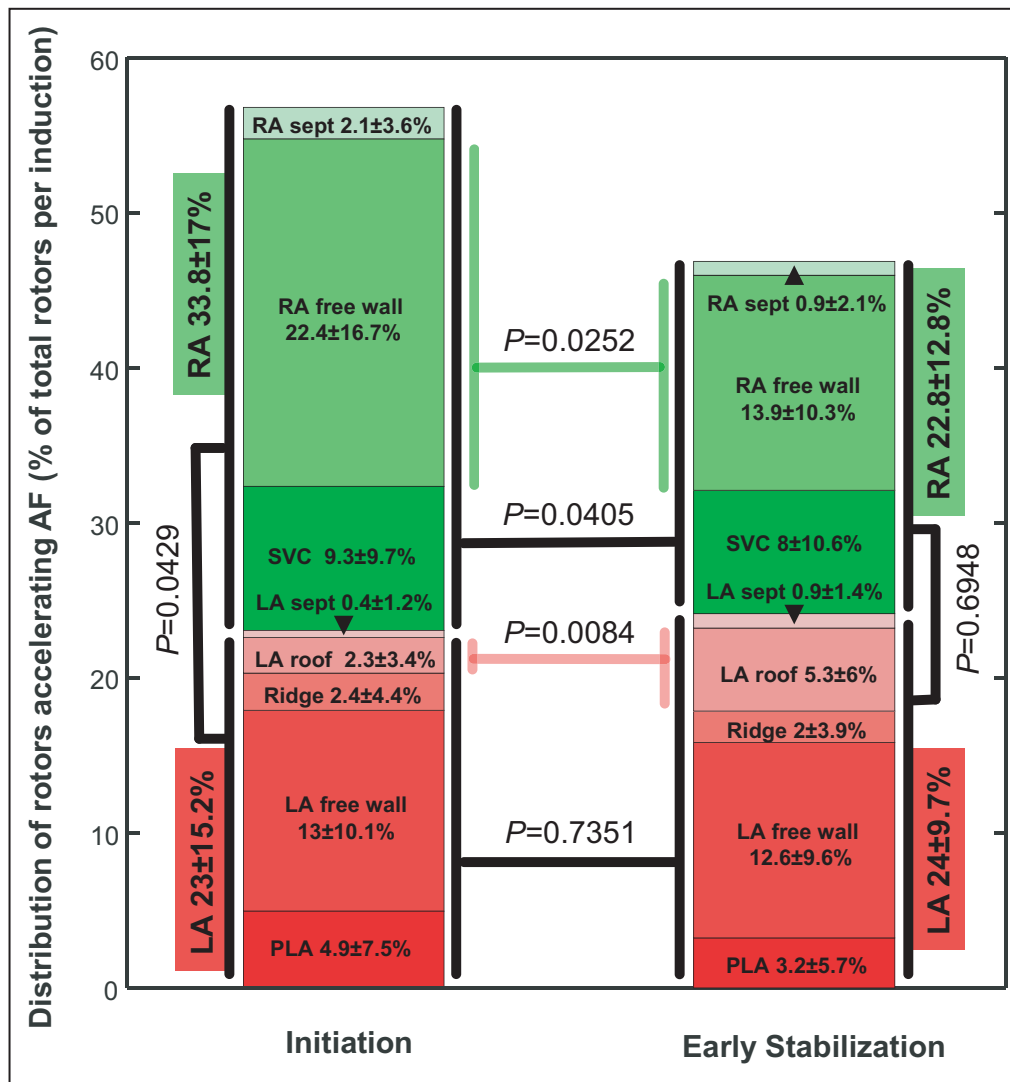
Figure 6. Regional distribution of rotors accelerating the atria.
Stacked bars show the amount of rotors in each region in cases where an atrial CLmin at their termination was less than the atrial CLmin at their appearance (red cases in Figure S11). Distributions are shown for Initiation and Early Stabilization. Regional rotors amounts are expressed as mean±SD percentage of 20 AF inductions in 5 hearts from the total number of atrial rotors analyzed during those Initiation and Early Stabilization stages (210 and 253 respectively). Comparisons were made by *t* test for normal distributions (Shapiro–Wilk test) and by Wilcoxon signed-rank test for nonnormal distributions. Statistical significance level is alpha=0.025 for dual comparisons. AF indicates atrial fibrillation; CLmin, 5% minimal cycle length; LA, left atrium; PLA, posterior left atrium; RA, right atrium; and SVC, superior vena cava.

deceleration at all stages of the AF onset (Figure 4B and Figure S12).

Mechanisms of Rotor-Induced Acceleration and Deceleration

During the AF onset, CL accelerations occurred when rotors were observed, but not all accelerations colocalized with the rotors. The CL abbreviation at the rotor sites has been proposed to be mediated by electrotonic effects abbreviating the APD near the core of the pivoting waves[29] reinforced in our cholinergic AF

model by the enhanced inward rectifier K^{+} currents.[30] Uninterrupted waves emanating from the rotor will abbreviate CL in its periphery (Figure 5A). In case of rotors drift as shown in Figure 5, the atria-wide activity may be further abbreviated via the Doppler effect[31] and advancement of local cycle phase of the rotating waves. However, the acceleration-deceleration fate of the postrotor atria-wide rate of activity may be the outcome of additional mechanisms related to rotors activations themselves as follows: On one hand, APDs and refractory periods shorten as membrane ionic currents adapt to fast rotor-induced activations and
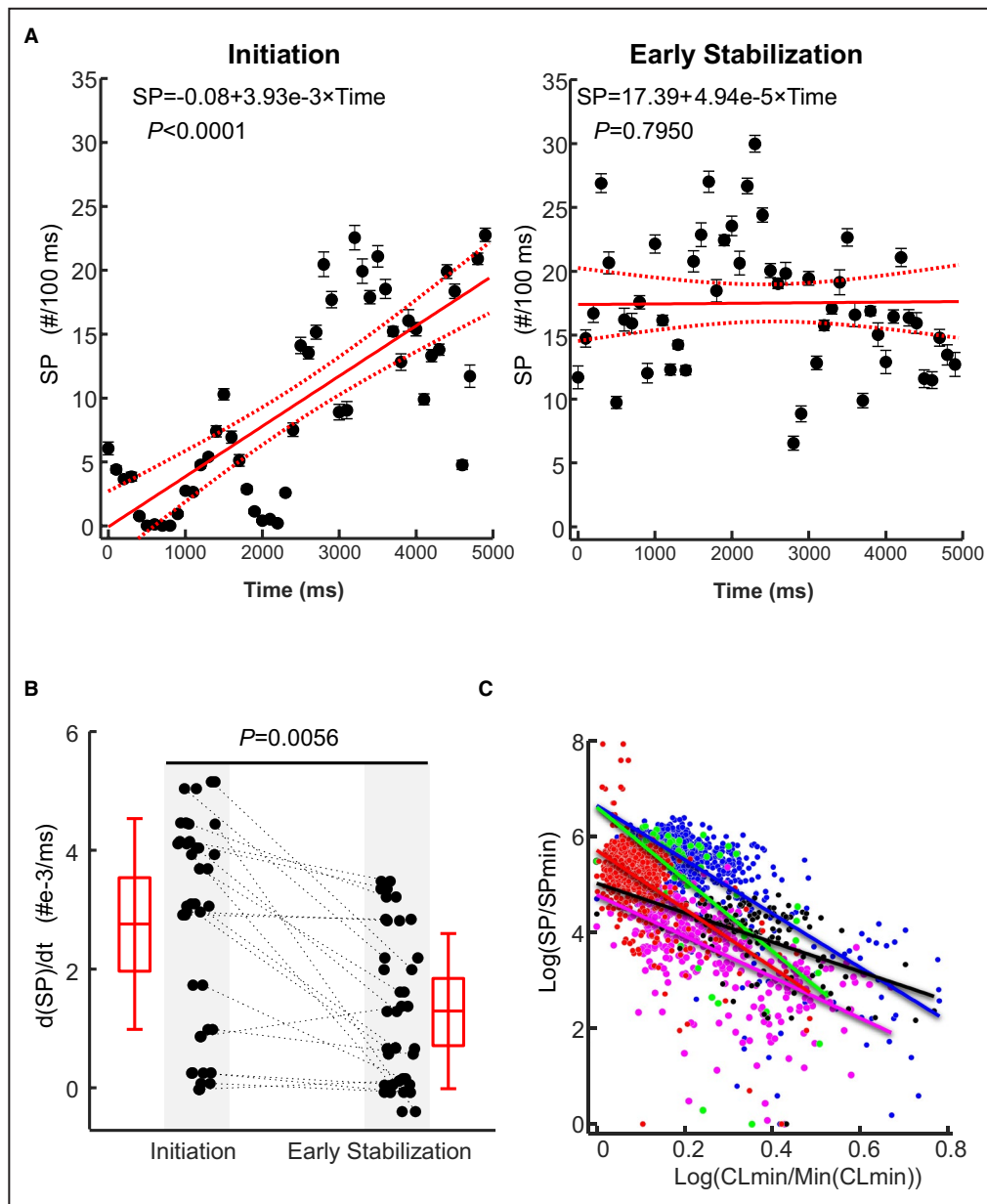
Figure 7. Time course of number of SPs during AF onset.
A, Representative example of number of SPs counted in bins of 100 ms during the Initiation (left) and Early Stabilization (right) stages of AF induction. Symbols show means and SDs of SPs per frame. Linear best fit formulas, lines and 95% CIs are superimposed on graphs. **B**, Summary of rate of change in SP numbers in 20 AF inductions in 5 hearts. Red markers indicate mean (horizontal bar), 95% CI of the mean (box) and SD (error bars) values. **C**, A logarithmic scatter plot between the number of SPs in 100 ms bins (n=1875) versus the CLmin in that bin for all 20 inductions in 5 separated hearts. SPmin=minimal number of SPs in a heart. Min(CLmin)=the minimal CLmin among all AF inductions in a heart. AF indicates atrial fibrillation; APD, action potential duration; BT, breakthrough pattern of impulse propagation; CL, cycle length; CLmin, 5% minimal cycle length; DF, dominant frequency; RA, right atrium; and SP, phase singularity point.

could remain abbreviated after the rotor termination by a memory effect.[32,33] On the other hand, computational studies on dynamics of rotors in the ionic heterogeneous atrial tissue have demonstrated that rotors slow down their rotation rate as they drift toward areas of lower excitability, which is also strongly affected by the spatial distribution of the inward rectifier current.[34] Noticeably, mechanisms underlying the opposing atrial acceleration and deceleration during and by rotors coexist and their net effect on the AF acceleration may

not require a continuous presence of rotors.[35] The panoramic optical mapping approach employed here, in combination with studies on ionic[14] and structural properties,[5,16,36] could be used to better elucidate on the acceleration rate across the atria during AF onset.

Clinical Implications

In clinical electrophysiology AF is defined when the arrhythmia lasts ≥30 s,[37] but 30-s long episodes have been consistently found[12] and anticoagulation is typically initiated once AF episodes of 30 s or longer are present,[38] highlighting the risk and the need to better understand, and possibly prevent, brief AF episodes as studied here. Our study can particularly shed light on the etiology of vagal-mediated paroxysmal AF, which is observed in the absence of detectable heart disease in young male adults.[39–41] In general AF in the clinic is often seen to initiate following focal activity from a varying origin.[2–4,6,42,43] The pulmonary veins have been described as the most common area of AF triggers,[2] but triggered activity has been observed elsewhere as well and pulmonary vein isolation, the most common clinical technique for AF ablation,[44] is suboptimal in terminating AF, and its efficacy is further reduced as AF progresses to persistent and permanent forms.[44,45] We find initial BTs and rotors across the 2 atria immediately following the premature pacing (Figures S3 and S4), consistent with the suggestion that discharges and driving activity can appear across the entire atria and in locations remote to the triggering event, which warrant a panoramic mapping. Our panoramic mapping further demonstrates that AF occurs following BTs and series of short lasting rotors, but only some of which associate with atria-wide acceleration. The possible presence of initial BTs and specific subsets of serial rotors contributing to the net result of atria-wide acceleration could potentially be a more specific target for improved ablative and nonablative therapies.

Limitations

The study investigates rotor dynamics during onset of AF in healthy isolated sheep hearts in the presence of 0.25 μmol/L carbachol. AF reentrant activity has been observed in other animal models and patients, under conditions such as increased intra-atrial pressure and presence of remodeling, and we cannot exclude different dynamics of acceleration in onsets of noncholinergic AF. The new wide-view lens used allows unprecedented panoramic mapping of endocardial surfaces. However, the optical mapping approach does not inform on activation patterns inside the thick myocardium and we also did not map the epicardial surfaces. As such, rotor activity and wavebreaks localized deeper than the subendocardial surfaces as well as on the epicardium and the distal portions of

the appendages and veins could not be detected and analyzed. Furthermore, because of the inability of our optical mapping approach to detect mid-myocardium and epicardial activity we cannot exclude the possibility that detected BTs represent the exit site of intramural reentries or wavebreaks. Finally, the differences found in the numbers of rotors with atria-wide acceleration versus deceleration actions, as well as in the net results of accelerations, are small and would benefit from additional confirmation studies.

CONCLUSIONS

A new system for panoramic and simultaneous optical mapping of the endocardial surfaces of the intact RA and LA provides the most comprehensive perspective on the dynamics of AF initiation to date. The new mapping system demonstrates that the DF increase during the onset of cholinergic AF in the sheep model correlates with a net result of opposing atria-wide acceleration-deceleration actions occurring concomitantly with rotors. The results suggest that the cumulative effect of drifting rotors, but not of multiple wavebreaks, could underlie the AF acceleration during its onset.

Supplementary Material

Data S1
Figures S1–S12
Videos S1–S6
References 46–49

REFERENCES

1. Heijman J, Guichard JB, Dobrev D, Nattel S. Translational challenges in atrial fibrillation. *Circ Res*. 2018;122:752–773. doi: 10.1161/CIRCR ESAHA.117.311081

2. Haissaguerre M, Jais P, Shah DC, Takahashi A, Hocini M, Quiniou G, Garrigue S, Le Mouroux A, Le Metayer P, Clementy J. Spontaneous initiation of atrial fibrillation by ectopic beats originating in the pulmonary veins. *N Engl J Med*. 1998;339:659–666. doi: 10.1056/NEJM199809 033391003

3. Kaneshiro T, Yoshida K, Sekiguchi Y, Tada H, Kuroki K, Kuga K, Kamiyama Y, Suzuki H, Takeishi Y, Aonuma K. Crucial role of pulmonary vein firing as an initiator of typical atrial flutter: evidence of a close relationship between atrial fibrillation and typical atrial flutter. *J Arrhythm*. 2017;33:86–91. doi: 10.1016/j.joa.2016.07.013

4. Cosio FG, Lopez-Gil M, Arribas F, Gonzalez HD. Mechanisms of induction of typical and reversed atrial flutter. *J Cardiovasc Electrophysiol*. 1998;9:281–291. doi: 10.1111/j.1540-8167.1998.tb00913.x

5. Klos M, Calvo D, Yamazaki M, Zlochiver S, Mironov S, Cabrera JA, Sanchez-Quintana D, Jalife J, Berenfeld O, Kalifa J. Atrial septopulmonary bundle of the posterior left atrium provides a substrate for atrial fibrillation initiation in a model of vagally mediated pulmonary vein tachycardia of the structurally normal heart. *Circ Arrhythm Electrophysiol*. 2008;1:175–183. doi: 10.1161/CIRCEP.107.760447

6. Schricker AA, Lalani GG, Krummen DE, Rappel WJ, Narayan SM. Human atrial fibrillation initiates via organized rather than disorganized mechanisms. *Circ Arrhythm Electrophysiol*. 2014;7:816–824. doi: 10.1161/CIRCEP.113.001289

7. Filgueiras-Rama D, Martins RP, Mironov S, Yamazaki M, Calvo CJ, Ennis SR, Bandaru K, Noujaim SF, Kalifa J, Berenfeld O, et al. Chloroquine terminates stretch-induced atrial fibrillation more effectively than flecainide in the sheep heart. *Circ Arrhythm Electrophysiol*. 2012;5:561–570. doi: 10.1161/CIRCEP.111.966820

8. Filgueiras-Rama D, Price NF, Martins RP, Yamazaki M, Avula UMR, Kaur K, Kalifa J, Ennis SR, Hwang E, Devabhaktuni V, et al. Long-term frequency gradients during persistent atrial fibrillation in sheep are associated with stable sources in the left atrium. *Circ Arrhythm Electrophysiol*. 2012;5:1160–1167. doi: 10.1161/CIRCEP.111.969519

9. Takemoto Y, Ramirez RJ, Kaur K, Salvador-Montanes O, Ponce-Balbuena D, Ramos-Mondragon R, Ennis SR, Guerrero-Serna G, Berenfeld O, Jalife J. Eplerenone reduces atrial fibrillation burden without preventing atrial electrical remodeling. *J Am Coll Cardiol*. 2017;70:2893–2905. doi: 10.1016/j.jacc.2017.10.014.

10. Lemola K, Chartier D, Yeh Y-H, Dubuc M, Cartier R, Armour A, Ting M, Sakabe M, Shiroshita-Takeshita A, Comtois P, et al. Pulmonary vein region ablation in experimental vagal atrial fibrillation: role of pulmonary veins versus autonomic ganglia. *Circulation*. 2008;117:470–477. doi: 10.1161/CIRCULATIONAHA.107.737023

11. Pandit SV, Zlochiver S, Filgueiras-Rama D, Mironov S, Yamazaki M, Ennis SR, Noujaim SF, Workman AJ, Berenfeld O, Kalifa J, et al. Targeting atrioventricular differences in ion channel properties for terminating acute atrial fibrillation in pigs. *Cardiovasc Res*. 2011;89:843–851. doi: 10.1093/cvr/cvq359

12. Steinberg JS, O'Connell H, Li S, Ziegler PD. Thirty-second gold standard definition of atrial fibrillation and its relationship with subsequent arrhythmia patterns: analysis of a large prospective device database. *Circ Arrhythm Electrophysiol*. 2018;11:e006274. doi: 10.1161/CIRCEP.118.006274

13. Berenfeld O, Mandapati R, Dixit S, Skanes AC, Chen J, Mansour M, Jalife J. Spatially distributed dominant excitation frequencies reveal hidden organization in atrial fibrillation in the Langendorff-perfused sheep heart. *J Cardiovasc Electrophysiol*. 2000;11:869–879. doi: 10.1111/j.1540-8167.2000.tb00066.x

14. Sarmast F, Kolli A, Zaitsev A, Parisian K, Dhamoon AS, Guha PK, Warren M, Anumonwo JMB, Taffet SM, Berenfeld O, et al. Cholinergic atrial fibrillation: $I_{K, AC}$h gradients determine unequal left/right atrial frequencies and rotor dynamics. *Cardiovasc Res*. 2003;59:863–873. doi: 10.1016/S0008-6363(03)00540-6

15. Berenfeld O, Efimov I. Optical mapping. *Cardiac Electrophysiol Clin*. 2019;11:495–510. doi: 10.1016/j.ccep.2019.04.004

16. Berenfeld O, Zaitsev AV, Mironov SF, Pertsov AM, Jalife J. Frequency-dependent breakdown of wave propagation into fibrillatory conduction across the pectinate muscle network in the isolated sheep right atrium. *Circ Res*. 2002;90:1173–1180. doi: 10.1161/01.RES.00000 22854.95998.5C

17. Kalifa J, Klos M, Zlochiver S, Mironov S, Tanaka K, Ulahannan N, Yamazaki M, Jalife J, Berenfeld O. Endoscopic fluorescence mapping of the left atrium: a novel experimental approach for high resolution endocardial mapping in the intact heart. *Heart Rhythm*. 2007;4:916–924. doi: 10.1016/j.hrthm.2007.03.009

18. Filgueiras-Rama D, Martins RP, Ennis SR, Mironov S, Jiang J, Yamazaki M, Kalifa J, Jalife J, Berenfeld O. High-resolution endocardial and epicardial optical mapping in a sheep model of stretch-induced atrial fibrillation. *J Vis Exp*. 2011:3103. doi: 10.3791/3103

19. Haissaguerre M, Hocini M, Denis A, Shah AJ, Komatsu Y, Yamashita S, Daly M, Amraoui S, Zellerhoff S, Picat M-Q, et al. Driver domains in persistent atrial fibrillation. *Circulation*. 2014;130:530–538. doi: 10.1161/CIRCULATIONAHA.113.005421

20. Lee G, McLellan AJ, Hunter RJ, Lovell MJ, Finlay M, Ullah W, Dhinoja MB, Sporton S, Earley MJ, Schilling RJ. Panoramic characterization of endocardial left atrial activation during human persistent AF: insights from non-contact mapping. *Int J Cardiol*. 2017;228:406–411. doi: 10.1016/j.ijcard.2016.11.085

21. Martinez-Mateu L, Romero L, Ferrer-Albero A, Sebastian R, Rodriguez Matas JF, Jalife J, Berenfeld O, Saiz J. Factors affecting basket catheter detection of real and phantom rotors in the atria: a computational study. *PLoS Comput Biol*. 2018;14:e1006017. doi: 10.1371/journ al.pcbi.1006017

22. Martinez-Mateu L, Romero L, Saiz J, Berenfeld O. Far-field contributions in multi-electrodes atrial recordings blur distinction between anatomical and functional reentries and may cause imaginary phase singularities - a computational study. *Comput Biol Med*. 2019;108:276–287. doi: 10.1016/j.compbiomed.2019.02.022

23. Rodrigo M, Guillem MS, Climent AM, Pedron-Torrecilla J, Liberos A, Millet J, Fernandez-Aviles F, Atienza F, Berenfeld O. Body surface localization of left and right atrial high-frequency rotors in atrial fibrillation patients: a clinical-computational study. *Heart Rhythm*. 2014;11:1584–1591. doi: 10.1016/j.hrthm.2014.05.013

24. Narayan SM, Jalife J. CrossTalk proposal: rotors have been demonstrated to drive human atrial fibrillation. *J Physiol*. 2014;592:3163–3166. doi: 10.1113/jphysiol.2014.271031

25. Guillem MS, Climent AM, Rodrigo M, Fernandez-Aviles F, Atienza F, Berenfeld O. Presence and stability of rotors in atrial fibrillation: evidence and therapeutic implications. *Cardiovasc Res*. 2016;109:480–492. doi: 10.1093/cvr/cvw011

26. Atienza F, Calvo D, Almendral J, Zlochiver S, Grzeda KR, Martinez-Alzamora N, Gonzalez-Torrecilla E, Arenal A, Fernandez-Aviles F, Berenfeld O. Mechanisms of fractionated electrograms formation in the posterior left atrium during paroxysmal atrial fibrillation in humans. *J Am Coll Cardiol*. 2011;57:1081–1092. doi: 10.1016/j.jacc.2010.09.066

27. Seitz J, Bars C, Theodore G, Beurtheret S, Lellouche N, Bremondy M, Ferracci A, Faure J, Penaranda G, Yamazaki M, et al. AF ablation guided by spatiotemporal electrogram dispersion without pulmonary vein isolation: a wholly patient-tailored approach. *J Am Coll Cardiol*. 2017;69:303–321. doi: 10.1016/j.jacc.2016.10.065.

28. Quintanilla JG, Alfonso-Almazan JM, Perez-Castellano N, Pandit SV, Jalife J, Perez-Villacastin J, Filgueiras-Rama D. Instantaneous amplitude and frequency modulations detect the footprint of rotational activity and reveal stable driver regions as targets for persistent atrial fibrillation ablation. *Circ Res*. 2019;125:609–627. doi: 10.1161/CIRCR ESAHA.119.314930

29. Beaumont J, Davidenko N, Davidenko JM, Jalife J. Spiral waves in two-dimensional models of ventricular muscle: formation of a stationary core. *Biophys J*. 1998;75:1–14. doi: 10.1016/S0006-3495(98)77490-9

30. Noujaim SF, Pandit SV, Berenfeld O, Vikstrom K, Cerrone M, Mironov S, Zugermayr M, Lopatin AN, Jalife J. Up-regulation of the inward rectifier

K+ current (I K1) in the mouse heart accelerates and stabilizes rotors. *J Physiol*. 2007;578:315–326. doi: 10.1113/jphysiol.2006.121475.

31. Davidenko JM, Pertsov AV, Salomonsz R, Baxter W, Jalife J. Stationary and drifting spiral waves of excitation in isolated cardiac muscle. *Nature*. 1992;355:349–351. doi: 10.1038/355349a0

32. Elharrar V, Surawicz B. Cycle length effect on restitution of action potential duration in dog cardiac fibers. *Am J Physiol*. 1983;244:H782–H792. doi: 10.1152/ajpheart.1983.244.6.H782

33. Cherry EM, Evans SJ. Properties of two human atrial cell models in tissue: restitution, memory, propagation, and reentry. *J Theor Biol*. 2008;254:674–690. doi: 10.1016/j.jtbi.2008.06.030

34. Calvo CJ, Deo M, Zlochiver S, Millet J, Berenfeld O. Attraction of rotors to the pulmonary veins in paroxysmal atrial fibrillation: a modeling study. *Biophys J*. 2014;106:1811–1821. doi: 10.1016/j.bpj.2014.02.030

35. Dharmaprani D, Schopp M, Kuklik P, Chapman D, Lahiri A, Dykes L, Xiong F, Aguilar M, Strauss B, Mitchell L, et al. Renewal theory as a universal quantitative framework to characterize phase singularity regeneration in mammalian cardiac fibrillation. *Circ Arrhythm Electrophysiol*. 2019;12:e007569. doi: 10.1161/CIRCEP.119.007569

36. Tanaka K, Zlochiver S, Vikstrom KL, Yamazaki M, Moreno J, Klos M, Zaitsev AV, Vaidyanathan R, Auerbach DS, Landas S, et al. Spatial distribution of fibrosis governs fibrillation wave dynamics in the posterior left atrium during heart failure. *Circ Res*. 2007;101:839–847. doi: 10.1161/CIRCRESAHA.107.153858

37. Fuster V, Ryden LE, Asinger RW, Cannom DS, Crijns HJ, Frye RL, Halperin JL, Kay GN, Klein WW, Levy S, et al. ACC/AHA/ESC guidelines for the management of patients with atrial fibrillation: executive summary a report of the American College of Cardiology/American Heart Association Task Force on Practice Guidelines and the European Society of Cardiology Committee for Practice Guidelines and Policy Conferences (Committee to Develop Guidelines for the Management of Patients With Atrial Fibrillation) developed in collaboration with the North American Society of Pacing and Electrophysiology. *Circulation*. 2001;104:2118–2150.

38. Garcia DA, Lopes RD, Hylek EM. New-onset atrial fibrillation and warfarin initiation: high risk periods and implications for new antithrombotic drugs. *Thromb Haemost*. 2010;104:1099–1105. doi: 10.1160/TH10-07-0491

39. Coumel P. Paroxysmal atrial fibrillation: a disorder of autonomic tone? *Eur Heart J*. 1994;15(suppl A):9–16. doi: 10.1093/eurheartj/15.suppl_A.9

40. Carpenter A, Frontera A, Bond R, Duncan E, Thomas G. Vagal atrial fibrillation: what is it and should we treat it? *Int J Cardiol*. 2015;201:415–421. doi: 10.1016/j.ijcard.2015.08.108

41. Estes NAM III, Madias C. Atrial fibrillation in athletes: a lesson in the virtue of moderation. *JACC Clin Electrophysiol*. 2017;3:921–928. doi: 10.1016/j.jacep.2017.03.019

42. Tsai CF, Tai CT, Hsieh MH, Lin WS, Yu WC, Ueng KC, Ding YA, Chang MS, Chen SA. Initiation of atrial fibrillation by ectopic beats originating from the superior vena cava: electrophysiological characteristics and results of radiofrequency ablation. *Circulation*. 2000;102:67–74. doi: 10.1161/01.CIR.102.1.67

43. Chen SA, Hsieh MH, Tai CT, Tsai CF, Prakash VS, Yu WC, Hsu TL, Ding YA, Chang MS. Initiation of atrial fibrillation by ectopic beats originating from the pulmonary veins: electrophysiological characteristics, pharmacological responses, and effects of radiofrequency ablation. *Circulation*. 1999;100:1879–1886. doi: 10.1161/01.CIR.100.18.1879

44. Kirchhof P, Benussi S, Kotecha D, Ahlsson A, Atar D, Casadei B, Castella M, Diener H-C, Heidbuchel H, Hendriks J, et al. 2016 ESC Guidelines for the management of atrial fibrillation developed in collaboration with EACTS. *Eur Heart J*. 2016;37:2893–2962. doi: 10.1093/eurheartj/ehw210

45. Page RL, Joglar JA, Caldwell MA, Calkins H, Conti JB, Deal BJ, Estes NA III, Field ME, Goldberger ZD, Hammill SC, et al. 2015 ACC/AHA/HRS guideline for the management of adult patients with supraventricular tachycardia: a report of the American College of Cardiology/American Heart Association Task Force on Clinical Practice Guidelines and the Heart Rhythm Society. *Circulation*. 2016;133:e506–e574.

46. Ramirez RJ, Takemoto Y, Martins RP, Filgueiras-Rama D, Ennis SR, Mironov S, Bhushal S, Deo M, Rajamani S, Berenfeld O, et al. Mechanisms by which ranolazine terminates paroxysmal but not persistent atrial fibrillation. *Circ Arrhythm Electrophysiol*. 2019;12:e005557. doi: 10.1161/CIRCEP.117.005557

47. Lalani GG, Schricker A, Gibson M, Rostamian A, Krummen DE, Narayan SM. Atrial conduction slows immediately before the onset of human atrial fibrillation: a bi-atrial contact mapping study of transitions to atrial fibrillation. *J Am Coll Cardiol*. 2012;59:595–606. doi: 10.1016/j.jacc.2011.10.879

48. Kneller J, Kalifa J, Zou R, Zaitsev AV, Warren M, Berenfeld O, Vigmond EJ, Leon LJ, Nattel S, Jalife J. Mechanisms of AF termination by pure sodium channel blockade in an ionically-realistic mathematical model. *Circ Res*. 2005;96:e35–e47.

49. Narayan SM, Baykaner T, Clopton P, Schricker A, Lalani GG, Krummen DE, Shivkumar K, Miller JM. Ablation of rotor and focal sources reduces late recurrence of atrial fibrillation compared with trigger ablation alone: extended follow-up of the CONFIRM Trial (Conventional Ablation for Atrial Fibrillation With or Without Focal Impulse and Rotor Modulation). *J Am Coll Cardiol*. 2014;63:1761–1768. doi: 10.1016/j.jacc.2014.02.543

SUPPLEMENTAL MATERIAL

Data S1.

SUPPLEMENTAL METHODS

This research was performed in accordance with the Unit of Laboratory Animal Medicine Policies, Guidelines and Standard Operating Procedures at the University of Michigan.

Langendorff perfused heart preparations

Five healthy male sheep weighing 30–40 kg were used in the study. The animal protocol was approved by the University Committee on Use and Care of Animals of the University of Michigan and conforms to the Guide for Care and Use of Laboratory Animals by the United States National Institutes of Health. Sheep hearts were isolated and Langendorff-perfused as described previously[7-9]. Briefly, following anesthesia induced by forelimb Propofol (4−6 mg/kg) IV administration, animals were heparinized (50 mg), intubated and ventilated. Thereafter, a midline sternotomy exposed the hearts which were quickly removed to result in a rapid death by exsanguination. Removed hearts were cannulated through the aorta and connected to a Langendorff-perfusion system with recirculating oxygenated Tyrode's solution at a flow rate of 200–240 mL/min (pH 7.4, 35.5–37.5°C). The composition of the Tyrode's solution was (mM): NaCl 130, KCl 4, $MgCl_2$ 1, $CaCl_2$ 1.8, $NaHCO_3$ 24, NaH_2PO_4 1.2, glucose 5.6 and albumin 0.04 g/L. After atrial transseptal puncture to equilibrate left and right atrial pressures, we ligated all orifices except the inferior vena cava which we cannulated with an outflow tube connected to a pressure transducer. Intra-atrial pressure was calibrated and controlled by adjusting the height of the outflow tube. Once connected, the ventricles were crated to keep the heart in a horizontal position with anterior aspects pointing upward and intra-atrial pressure maintained at 5 cm H_2O for the duration of the experiment to mimic diastolic left atrial pressure. Electrodes continuously collected bipolar recordings from the left and right atrial epicardium for rhythm monitoring. We ensured that the heart was in healthy sinus rhythm at the beginning of each experiment and then administered a bolus of blebbistatin (10–20 μM, Enzo Life Science, NY, USA) and induced ventricular fibrillation to abolish motion artifacts in the atria during optical mapping.

AF inductions

AF onset, including initiation and early stabilization periods, were studied following the addition of 0.25 μM carbachol to the circulating perfusate[10,11]. AF was induced with an S1-S2 programmed pacing protocol as follows: 10 S1 stimuli at twice the capturing amplitude were administered at 300 msec intervals and an S2 extra-stimulus was administered from the LA free wall at progressively shorter coupling interval until AF was induced or tissue became refractory. For this study, induced AF episodes were classified as self-sustained if lasted at least 40 sec[12]. Longer AF episodes were cardioverted by bi-atrial electric shock and hearts permitted to stabilize in sinus rhythm before repeating the AF induction pacing protocol. Up to about 30 trials of AF inductions were conducted in each heart. The S1-S2 induction protocol guarantees no external stimulus is present during the Initiation and Early

Stabilization periods. Sixteen randomly selected non-sustained episodes and all 20 sustained AF episodes were included in the analysis. Analysis is focused on two periods of the AF onset: The first 7 sec period post S2 is termed here the Initiation period and the 10 sec period 30 sec post S2 is termed here the Early Stabilization period.

Wide-view endoscopic optical mapping (Figure S1)

The novel wide-view endoscopic mapping approach used in this study is illustrated in Figure S1. The approach builds on a new objective lens unit comprising of negative and correcting lenses assembly designed to extend the original borescope field of view when immersed in the translucent Tyrode's solution filled atrial cavities. Panel A shows the basic optical properties of the developed wide-view objective lens unit demonstrated by imaging the inside of a 75 mm diameter sphere with multiple uniform size holes of 11 mm in diameter each using the same system as in the experiments. The center of the right image (green circle) is the sphere point farthest from the objective lens and the periphery of the image corresponds to the sphere area nearest to the lens. The lens projection of the spherical surface onto the image is accomplished by local scale transformation whereby the radial axis is contracted and the angular axis is stretched from the center to the periphery of the image. At the periphery, about 37 pixels from the center of the image, the 11 mm circular hole (yellow ellipse) is seen to be radially contracted by 40% (orange lines) and angularly stretched by 35% (cyan lines).

For imaging the endocardial surfaces of the atria lesions were cut at left ventricular apex and right ventricular free wall to enable insertion of two dual-channel solid borescopes (Everest VIT, GE Inspection Technologies, Huerth, Germany) toward the left and right atria (panel B). The distal ends of the borescopes were equipped with new wide-view objective units and advanced through the ventricular lesions to position the objective unit at the plane levels of the left and right atrioventricular valves, thus enabling viewing the entire endocardial atrial surfaces. The geometrical shape of the atria chambers is complex and variable, but its general concave shape relative to the objective lens renders the endocardial wide-view optics with less geometrical distortions as compared with a wide-view image of flat or convex surfaces. Color images at ambient light taken via the borescopes in its mapping position are showing panoramic internal views of the atria, including their septa, roofs, vena cava, pulmonary veins and the free walls (panel C). The system is imaging the proximal aspects of the appendages (which are shallower in sheep than in humans).

Following the positioning of the borescopes and their objectives, the lesions were sealed to maintain a stable intra-atrial pressure and the proximal ends of the borescopes were coupled to two synchronized 14 bits CCD cameras (SciMeasure, Decatur, GA) on the acquisition channels, and to two light guides delivering 532 nm excitation light on the illumination channel[8,17,18]. The two cameras and borescopes were then used to record voltage-sensitive di-4-ANEPPS fluorescence from the endocardial surfaces of the two atria in 10 sec long movies of 80×80 pixels each at 600 frames/sec. Movies of the right and left atria were filtered in time and space and their background intensity subtracted to yield the dynamic time series

of the fluorescence as previously performed[7-9]. Panel D of Figure S1 shows background intensity images from a representative heart marked with locations of 4 sample fluorescence traces during AF shown in panel E. As can be appreciated from the traces, the amplitude of the signals varies between recording sites; however, at a minimum of about 100 arbitrary digital units levels of fluorescence the cycles of the AF activation waves are clearly detectable[17]. Sample videos are provided as Videos S1-S6.

Optical data analysis

Analyses included spatial and temporal quantifications of phase-, frequency- and time-domain parameters[18,46] as follows:

Phase-domain analysis: The action potentials phase in each pixel was computed using the Hilbert transform. In phase maps, propagation is from high to low phases modulo 2π. Phase singularity points (SPs) in maps, defined as a location towards which all phases converged, were identified manually and their time and coordinates marked blind to subsequent analyses. All marked SPs were included in analyses. Rotors were defined as waves pivoting around an SP for >1 cycle. SPs of rotors were tracked to determine their trajectory and lifespan. SPs lasting less than one rotation were considered wavebreaks.

Frequency-domain analysis: Fluorescence movies were divided into 3-sec long segments for analysis of the time-course of the dominant frequency (DF) defined as the frequency with the maximum power at each pixel in each segment. We defined maximal DF (DFmax) in DF maps as the highest DF present in >20 contiguous pixels.

Time-domain analysis: For fluorescence time-series of each pixel, up- and down-strokes were automatically detected between peaks and the cycle length (CL) was calculated as the time interval between 50% of peak-to-peak amplitudes in sequential upstrokes[46]. CLs of all pixels formed a new movie whereby each frame presented the atria-wide CLs for each pixel during the duration of each cycle.

Cycle length analysis: CLs in two locations and settings were collected from frames of the CL movies: (i) The CLs at the rotors sites before and during the rotor SP appearance were used to determine the rotor-induced CL changes at the rotors sites themselves. Signals at rotors' cores may have low amplitude hence a CL at a coordinate of interest was determined by averaging values from a 3×3 pixels array centered at that coordinate in the CL maps. (ii) The minimal CL (CLmin) >5 percentile anywhere in the atria was used to determine the atria-wide fastest activation rate at a given moment.

Acceleration and deceleration: Reduced or increased values of CL in time at rotor-site and CLmin across the atria are considered acceleration or deceleration, respectively, at their corresponding locations. CL at rotor sites was evaluated before and during the rotor presence to study the effect of rotor formation on local acceleration or deceleration. Atria-wide CLmin values at movie frames immediately before and after rotor SPs presence, and

100 msec after a non-rotor SPs presence, were used to study the acceleration or deceleration effects of rotors and non-rotors SPs on the fastest activation rate in any location across the entire atria.

Action potential duration: For fluorescence time-series of each pixel during pacing activity, up- and down-strokes were automatically detected. Action potential duration at 70% repolarization (APD_{70}) was calculated for each pixel between 50% peak-to-peak upstroke level and subsequent down-stroke at 70% peak-to-peak repolarization level.

Rotor drift distance and velocity: The start and finish pixel sites of the SPs trajectory of a rotor were used to determine its begin-to-end drift vector. For each rotor, the drift vector was decomposed into its radial and angular components which were multiplied by a factor of $1+0.4R/37.3$ and $1-0.35R/37.3$ respectively to account for the panoramic optical projection distortion (R being the distance between the center of the vector and the center of image in pixels; see Figure 1A). The magnitude of the drift vector following a multiplication by a conversion factor of 1.859 was considered the drift distance expressed in millimeters. The rotor drift velocity was then calculated by the ratio of the drift distance to the rotor lifespan. As the rotor drift distance and velocity were calculated from the begin and end flanking points of the SP drift trajectory, they refer to the effective whole rotor drift and not to the meandering of its instantaneous SP location.

SUPPLEMENTAL RESULTS

Atrial activation during pacing (Figure S2)

The distribution of atrial action potential duration at 70% repolarization (APD_{70}) across the RA and LA was analyzed during the S1 pacing stimuli at 300 msec intervals prior to the premature stimulus (see Supplemental Methods and Figure 1) and is presented in Figure S2. Figure S2A shows the endocardial RA and LA panoramic activation time (ACT) map of the last of the 10 S1 waves paced at 300 msec intervals in the same heart shown in Figure S1 (see also Video S1). Pacing was from the LA free wall (asterisk) and the ACT map shows an uninterrupted propagation toward the RA with a complete bi-atrial conduction time of approximately 75 msec[47]. The APD_{70} for averaged S1 waves in the same representative heart was 109.7±7.4 msec for the RA and 96.2±13.3 msec for the LA. We further analyzed the regional and whole atria APD_{70} distribution measured in 19 movies of S1 waves paced at 300 msec intervals and preceding inductions of sustained AF in 5 hearts (Figure S2B). We found that APD_{70} varied across the various bi-atrial anatomical regions (Two-way ANOVA test p<0.0001) and averaged APD_{70} for all RA regions was longer than the for all LA regions (112.6±19.3 msec vs. 93.9±9.9 msec respectively, p<0.0001)[48].

Initial breakthroughs and rotor activation patterns (Figures S3 and S4)

Breakthrough (BT) of an initiating wave and repeat pivoting rotor patterns of activity are of particular interest as possible drivers and targets in ablation to terminate AF[19,49]. Both patterns were observed in our experiments (Figure S3A) here and we first characterize them

during the period immediately following the S2 extra stimulus. Panel A of Figure S2 shows sample phase snapshots of BT and rotor patterns in an AF induction; immediately subsequent to the S2 wave a radial wave propagation from a BT activation is demonstrated in the area between the ridge and free wall of the LA; immediately thereafter, a single counterclockwise rotational activity is seen around an SP at the SVC area; about 30 sec later, multiple SPs indicating either wavebreaks or rotor activity are seen throughout both atria (see Figure S3).

Analysis of 20 sustained AF inductions showed that the first activation patterns following the S2 wave were BTs in 16 (80%) and rotors in 4 (20%) cases (Figure S3B). The first BTs were 13/16 in the LA and 3/16 in the RA. In all the inductions that resulted in sustained AF, rotors followed the BT activity with the first ones appearing mostly in the RA; 13 times in the RA, 4 in the LA and in 3 cases they appeared simultaneously in the RA and the LA (Fisher's exact test two-tailed p=0.0081).

The sequence of BTs appeared sometimes at an alternating atrium and could not be linked to each other in space. We however characterize the time intervals between sequential BTs of new waves to better understand their possible role in the AF onset. Figure S3C is a scatter plot of the BT intervals vs. the cycle number in the sequence (first interval is between the S2 and the first BT waves) for inductions leading to sustained (red) or non-sustained (blue) AF. The plot reveals large scattering of BT intervals, however a linear regression analysis demonstrates a separation between the non-sustained AF and sustained AF; inductions whose activity resulted in non-sustained AF (n=16) showed no significant trend in BT intervals over time (blue, y=0.9x+123.9 msec, R^2=0.0119, p=0.368) and inductions whose activity resulted in sustained AF (n=20) showed decreasing BT intervals over time (red, y=-4.3x+113.6 msec, R^2=0.0309, p=2.63e-4). The analysis in Figure S3 and the sample sequence of phase maps in Figure S4 demonstrates that our mapping of the activation patterns during the initial stage of the sustained AF reveals BTs activity that accelerates and transforms into rotational activity.

Inductions not resulting in sustained AF (Figure S5)

A sample of phase movie snapshots during an induction that failed to result in a sustained AF is shown in Figure S5. One hundred sixty-four msec after the S2 stimulus in the LA, a first non-paced activation wave is seen to originate in a BT in the RA and to propagate uninterrupted across the RA and the LA. A 2nd non-paced similar activation pattern originating in a BT in the RA is seen at 287 msec after S2 (123 msec BTs interval). Following additional 2 BT activations (not shown), a 5th and 6th BT activation patterns are visible at 680 and 829 msec post S2, respectively (159 msec BTs interval). Overall, the 4 patterns of activations during the 6 non-paced BT waves presented in Figure S5 do not show SPs at any time and are followed by a period of quiescence, shown at a sample 977 msec snapshot. Subsequently to the non-activation period, 936 msec after the 6th BT activity, sinus rhythm was resumed as seen by the first sinus wave originating at a BT in the RA illustrated at 1765 msec post-S2.

Time-course of regional distribution of rotor presence (Figure S6)

The regional distribution of rotor appearance during the Initiation and Early Stabilization stages is presented in Figure S6 following these steps: First, all SPs belonging to rotors were annotated for the region were they appear in each movie frame. Second, for each region the number of SPs in 10,000 frames (16.7 sec) were counted separately for the Initiation and Early Stabilization stages. Third, the percentage of rotor presence in each region was calculated as the ratio of the counted number of SPs for that region to the total number of SPs counted for all the regions. And finally, the regional percentages for the 20 AF inductions were averaged and presented as stacked bar columns.

Thus, Figure S6 presents a quantification of the time with rotational activity lasting more than one cycle across all RA and LA regions, expressed as the percentage of the total time with rotational activity anywhere and anytime, separately during Initiation (left column) and during Early Stabilization (right column). The SPs of a total of 572 rotors were tracked in 30,695 frames (about 51.2 sec) during Initiation and 45,211 frames (about 75.3 sec) during Early Stabilization. During Initiation, there was a trend for SPs of rotors to be more abundant in the RA (55.8±18.9%) than in the LA (44.2±18.9%; p=0.0621). As AF progresses to Early Stabilization, we observed a significant shift in the amount of rotors presence only in two areas: The LA roof rotors presence increased from 5.7±6.1% to 10.7±10.5% (p=0.0187) and the RA free wall decreased from 35.5±18.7% to 25.6±16% (p=0.0121). Overall, during the transition to Early Stabilization the RA rotors presence tended to decrease from 55.8±18.9% to 44.3±23.9% and LA rotors presence tended to increase from 44.2±18.9% to 55.7±23.9% (p=0.0670), practically reversing the rotors presence distribution during Initiation to have less RA rotors than LA rotors during Early Stabilization, but not to a significant level (p=0.1364). Please note that RA and LA percentage values are complementary to 100% for reach induction and therefore their STD values, as well as the t-test p values characterizing the transition from Initiation to Early Stabilization, are identical. In addition, the value of Alpha may be adjusted to 0.025 to determine the significance of the between RA and LA differences and transitions from Initiation to Early Stabilization observed in this analysis.

Time-domain acceleration of activity (Figure S7)

For greater insight into the dynamic process of acceleration we generated CL movies of beat-by-beat activation intervals for all pixels. For each movie frame (instantaneous CL map) we selected the minimal CL (CLmin) and analyzed the time course of CLmin in binned periods of 166 msec (100 frames). Figure S7A shows the time course of CLmin during Initiation (left) and Early Stabilization (right) stages of a sample induced AF. Linear best fit shows an acceleration trend (reduction of CLmin) during Initiation (p<0.0001) contrasted by a constant CLmin during Early Stabilization (p=0.8435). Composite analysis of 20 inductions of sustained AF is presented in Figure S7B. The linear regression intercept (left) indicates the CLmin at the beginning of the two stages decreased from 71±25 to 57±16 msec (p<0.0001); the linear regression slope (right) indicates the CLmin trends during the two

stages is increasing from -1.65 ± 2.2 to 0.04 ± 0.02 ($\times 10^{-3}$, p=0.0019). Overall, the gradual reduction in CLmin during Initiation and its eventual steadiness later during Early Stabilization parallels the time course of DFmax shown in Figure 2B.

Time-course of regional DFmax distribution (Figure S8)

Figure 2 of the manuscript describes the time course of the DFmax across the entire atria during the AF onset. Here we describe in Figure S7 in more details the time-course of the DFmax specific to each of the atria regions as outlined in the anatomical diagrams in Figures 2, S2 and S3. DFmax data for 20 AF inductions presented in Figure S8 show a variability across the different regions and times. On average the PLA (red symbols) is hosting the DFmax during all 4 periods of time analyzed, albeit not always significantly higher than the other regions. The corresponding average values of the DFmax at the PLA are 11.11±0.58 Hz (0-3 sec, p=0.0586), 13.03±0.58 Hz (4-7 sec, p=0.5764), 15.13±0.58 Hz (30-33 sec, p=5.2e-05) and 14.67±0.58 Hz (37-40 sec, p=0.0675). Interestingly, the average DFmax at the SVC (green symbols) region is second highest and not statistically different from the highest DFmax at the PLA at the 0-3 and 37-40 periods (11.08±0.67 Hz; p=0.9279 and 14.22±0.71 Hz; p=0.6012, respectively). It is also interesting to note that despite the PLA presenting the highest average DFmax in each period, on an individual induction basis, the other LA regions of the ridge, the free wall and the roof (red arrows) presented similar or higher DFmax values. Finally, the higher average DFmax values in the LA free wall as compared with the RA free wall (blue and dark green symbols, respectively) over the 4 time periods analyzed in Figure S8 is consistent with previous epicardial optical mapping studies of cholinergic AF in isolated sheep heart showing also that the LA free wall was activated at a faster DF than the RA free wall[14].

Time-course of rotors appearance and lifespan (Figure S9)

The CLs localized to rotor sites, at cycles prior and during the rotors presence and identified in 20 inductions of AF, were collected using the tracking method shown in Panel A of Figure 3. A total of 217 and 357 rotors detected during Initialization and Early Stabilization stages, respectively were analyzed in Figure S9 for appearance rate and time lifespan in each consecutive 1 sec long bins of time. ANOVA tests revealed that there were no significant differences between inter-bin rates of appearance at the two stages (Panel A; left, p=0.4743 and right, p=0.1253, respectively) and rotors appeared in the 20 inductions in series at 5 sec average rates of 2.0±1.37 vs. 3.29±2.09 rotors/sec during Initiation and Early Stabilization, respectively (p<0.0001). The number of rotors detected decreased with their number of lifespan cycles before disappearance, as in previous studies[14], and they completed up to 6 cycles during Initiation and up to 10 cycles during Early Stabilization before dissipating. Although the 5 sec average number of their cycles lifespan in the 20 inductions was similar (1.75±1.03 vs. 1.76±1.2 rotations per rotor; p=0.9048; not shown), their 5 sec average time lifespan decreased from 224.1±118.8 to 196.6±110.4 msec, respectively, (p=0.0074. Panel B). ANOVA tests on inter-bin time lifespan of rotors in Panel B revealed significant variability during Initiation (left, p=0.0062) and non-significant variability during Early Stabilization

(right, p=0.5423), providing another parametrization for the dynamic activation process of AF onset in our model.

Reduction and increase of atrial CLmin during rotors and non-rotors SPs (Figures S10-S12)

Both accelerations and decelerations of the activity across the atrial were observed during the presence of rotors and non-rotors SPs. Figure 4A shows a sample case in which the LA-wide minimal CL is reduced following a rotor appearance and disappearance (acceleration). In Figure S10 we show an opposite sample case in which the LA-wide CLs are prolonged (deceleration) following the presence of a rotor. The sample pixel signal in Figure S10 is showing that the 2 CLs before the rotor appearance are 75 and 72 msec and following the rotor disappearance the CLs shown prolong to 84 and 92 msec. The corresponding LA-wide CL maps show a general prolongation of CLs with increasing areas of CLs >140 msec (red-yellow areas). We analyzed the cumulative contribution of rotors and non-rotors SPs presence on the CLs across the entire two atria to provide insight on the transition of the AF from accelerating during Initiation to stable activation rate during Early Stabilization, despite the constant acceleration of activity at the rotor site during the two AF stages as shown in Figure 3B.

The CLmin values across the entire atria varied greatly between different inductions and stages of AF and are analyzed in Figures S11 and S12. In Figure S11, CLmin prior to rotors were compared with CLmin subsequent to the same rotors. We analyzed changes in atria-wide CLmin values for 210 rotors during Initiation, and 362 rotors during Early Stabilization. The post-rotor CLmin decreased compared to pre-rotor CLmin in 113 (53.8%) of cases during Initiation and 156 (43.1%) of cases during Early Stabilization. During Initiation (left, n=210), the 113 pairs demonstrating acceleration showed CLmin reduction of -20±18.9 msec and the 97 pairs demonstrating deceleration showed CLmin increase of 16.4±15.5 msec (Wilcoxon test p<0.0001). Overall, the effect of all rotors analyzed during Initiation demonstrated a cumulative CLmin shortening from 90.2±32.3 msec to 87.3±33 msec (paired t-test p=0.0439). During Early Stabilization (right, n=362), the 156 pairs demonstrating acceleration showed CLmin decrease of -15.2±13.7 msec and the other 206 pairs demonstrating deceleration showed CLmin increase of 14±13.9 msec (Wilcoxon test p<0.0001). Overall, the effect of all rotors analyzed during Early Stabilization demonstrated a non-significant cumulative CLmin alteration from 77.6±26 msec to 78.7±26.9 msec (paired t-test p=0.1671). Aggregate analysis of the pairs of CLmin values during Initiation and Early Stabilization showed there was a significant average atria-wide reduction by -3.5±25.2 msec (p=0.0439) during each rotor at Initiation, and a non-significant average atria-wide increase by 1.2±20 msec (p=0.1671). Thus, the rotors presence is associated with atria-wide acceleration of AF at Initiation versus stability of AF rate at Early Stabilization (p=0.0112).

In contrast to the effect of rotors, the non-rotor SPs was not associated with reduction of the atria-wide CLmin. In Figure S12 pairs of CLmin values immediately prior and subsequent to 313 non-rotor SPs during Initiation and 696 non-rotor SPs during Early Stabilization were

compared after normalization to the earliest CLmin in each movie to account for the large variability across pairs from different inductions. Differences between normalized mean values of pre-SP and post-SP CLmin were less than 1% during both Initiation (p=0.583) and Early Stabilization (p=0.235). The normalized CLmin differences also did not differ between Initiation and Early Stabilization (p=0.4497). Thus, only the cumulative activity of accelerating rotors, and not non-rotor SP presence in general, is associated with acceleration of AF during onset.

Figure S1. Experimental setup and panoramic data.
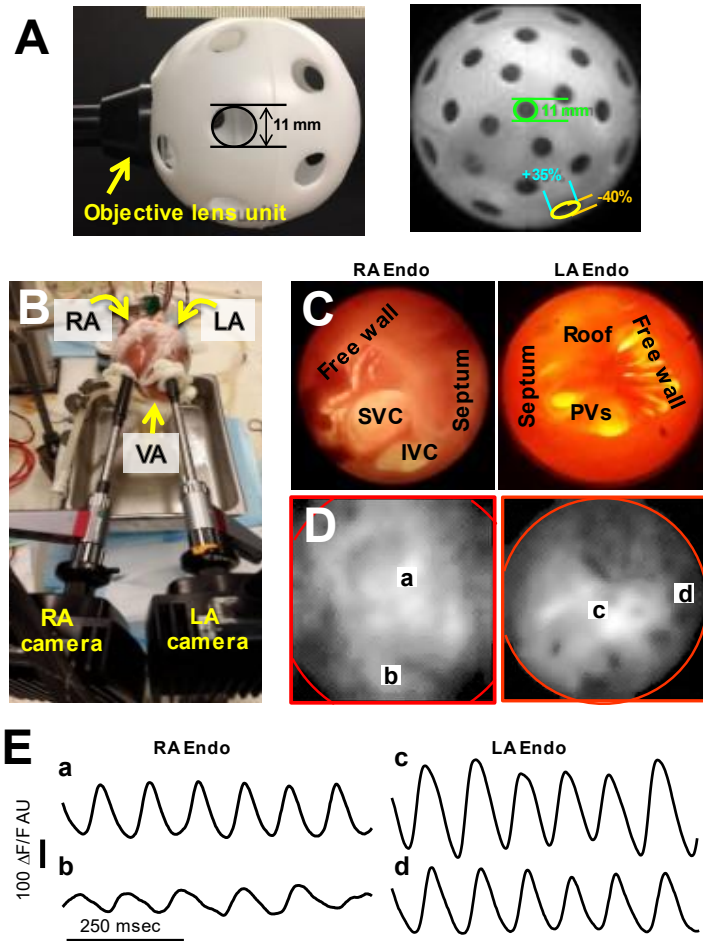
A) Basic properties of the new wide-view lens unit demonstrated in viewing the inside of a training baseball ball of about 75 mm in diameter. Left: The developed wide-view objective lens unit is attached to a borescope and a CCD camera as described below and is placed inside a spherical 75 mm diameter training baseball ball with circular holes (11 mm diameter) for scaling of the inside view. Top ruler scale is in mm. Right: Circular holes of the sphere are visible through the wide-view lens and the camera system. The central 11 mm diameter hole (green circle) is the farthest from the lens and the peripheral holes (yellow ellipse) are the closest to the lens. The projection of the sphere on the image is accomplished by a radial contraction and angular stretch of the periphery relative to the center of the image. At the periphery, 37.3 pixels from the center of the image, the 11 mm circular hole (yellow ellipse) is seen to be radially contracted by 40% (orange lines) and angularly stretched by 35% (cyan lines). **B)** View of the experimental setup showing the two cameras (bottom of image) attached to two borescopes equipped with wide-view objective lenses inserted through the ventricles' apexes (VA) to map the RA and LA in the

Langendorff perfused isolated sheep heart (top of image). **C)** Visual color image of the endocardial surfaces of the RA (left) and LA (right) obtained via the borescopes and the wide-view lenses. **D)** Sample background fluorescence intensity images of the two atria obtained with the cameras in B. **E)** Sample traces of dynamic fluorescence obtained in pixels marked in D. Amplitude of signals exceeded 100 arbitrary digital units.

Figure S2. Atrial action potential duration during S1 pacing.
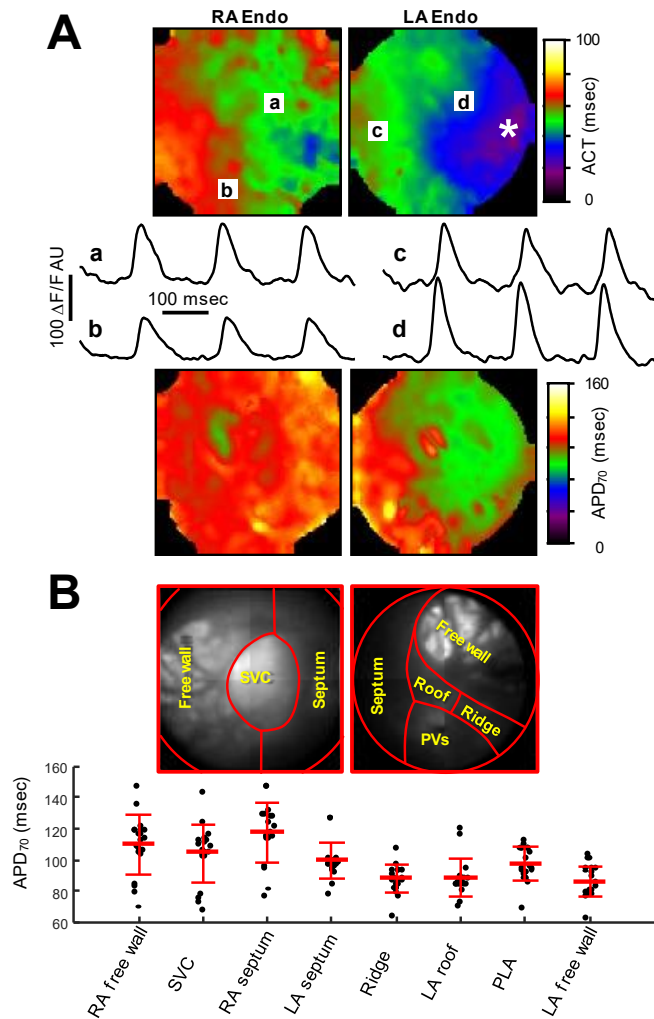
A) Top: Endocardial RA and LA panoramic activation time (ACT) map during the last of 10 S1 paced waves (at 300 msec intervals) in the same heart shown in Figure S1. Pacing is from the LA free wall (asterisk). Middle: Representative single pacing recordings during the last 3 S1 waves are shown. Bottom: APD_{70} map for the averaged S1 waves in the same heart. RA APD_{70} is 109.7±7.4 msec and LA APD_{70} is 96.2±13.3 msec. **B)** Top: A representative endocardial image and outline of 8 anatomical RA and LA regions. Please note that the inferior vena cava as well as the distinction between the left and right pulmonary veins (PVs) in the sheep atria are not visible in some cases and we therefore combine their data into unifying superior vena cava (SVC) and PVs regions, respectively. Bottom: The individual, mean and STD APD_{70} for the anatomical regions outlined measured during S1 pacing preceding inductions of sustained AF (N=5, n=19). APD_{70} varies across regions

(Two-way ANOVA test p<0.0001) and APD_{70} for all RA regions is longer than the for all LA regions (112.6±19.3 msec vs. 93.9±9.9 msec respectively, p<0.0001)[48].

Figure S3. Initial activation patterns and their progress.
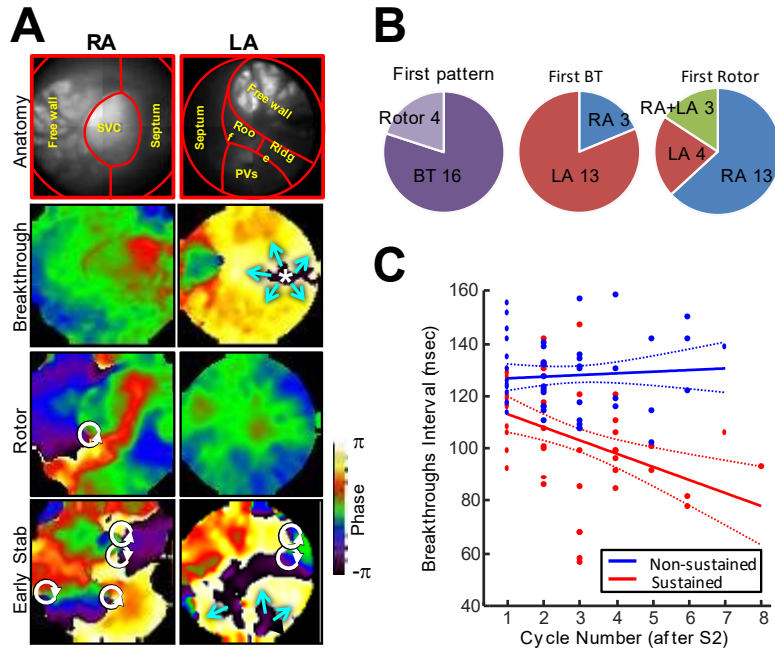
A) Anatomy image and activation patterns in a sample AF induction panoramic mapping of the RA and LA endocardial surfaces. From top to bottom panels: (i) The anatomy image of the panoramically mapped RA and LA (SVC, superior vena cava; PVs, pulmonary veins). (ii) A breakthrough (BT, asterisk) pattern at the edge of the LA free wall region during initiation of AF. (iii) A rotor pattern is followed in the RA. (iv) During early stabilization, a complex activation includes multiple reentries and BTs across both atria. **B)** Patterns of activity in 20 self-sustained AF inductions in N=5 hearts. Left: Incidences of BTs and rotors as first activity after S2. Center: Location of first BTs after S2. Right: Location of first rotor, either immediately after S2 or after BTs. Two-tailed Fisher's exact test: p=0.0081. **C)** Linear regression analysis of cycle length (CL) between sequential BTs following S2 vs. the BTs cycle number in non-sustained AF inductions (blue, N=5, n=15) and sustained AF inductions (red, N=5, n=20). F-test for linear comparisons: p=0.006.

Figure S4. A sequence of phase movie snapshots during a representative AF induction.
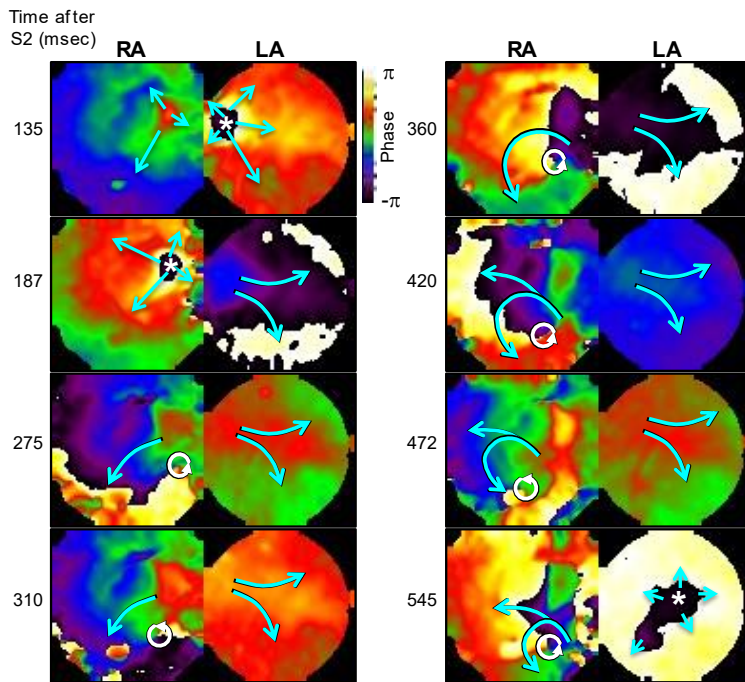

One-hundred thirty-five msec after the S2 pacing in the LA (not shown), a new wave breakthrough endocardial (BT, asterisk) appears in the LA septal area with a delayed BT in the RA. Following, at 187 msec, another BT appears at the RA with a delayed BT in the LA. Thereafter an SP is formed in the RA and becomes a rotor that lasts for more than one rotation (snapshots at 275 to 545 msec). The concomitant activity in the LA is regular with BTs at all snapshots. Arrowhead circles: location and chirality of a rotor.

Figure S5. A sequence of phase movie snapshots during an induction that failed to result in a sustained AF.
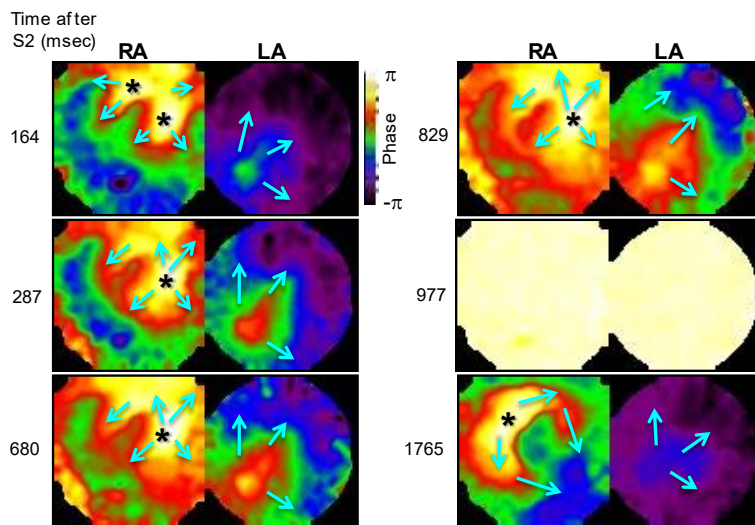

One hundred sixty-four msec after the S2 stimulus in the LA, a first non-paced activation wave is seen to originate in an RA breakthrough (BT, asterisk) and to propagate uninterrupted across the RA and the LA. A 2nd non-paced similar activation pattern originating in a BT in the RA is seen at 287 msec after S2. Following additional 2 BT activations (not shown), a 5th and 6th BT activation patterns are visible at 680 and 829 msec post S2, respectively. Subsequently, a period of quiescence pause in activity across the RA and LA is presented at 977 msec post S2, which is followed by a sinus rhythm wave originating at a BT in the RA presented at 1765 msec post S2.

**Figure S6. Rotor distribution across atrial regions.**
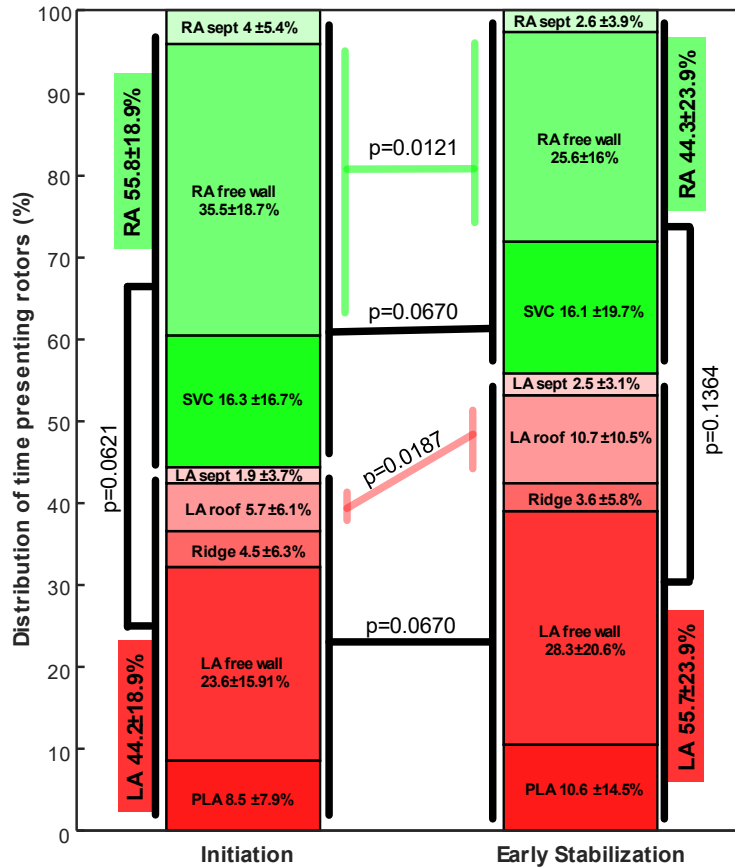
Stacked bar representation of percentage of time that the rotors existed in each of the atrial regions at Initiation (left) and Early Stabilization (right) of AF. Numbers for each region represent the mean±STD percentage time rotors were present in that region relative to all rotors (in all regions and all times) in the 20 inductions (N=5, n=20; total number of rotors at Initiation was 216, total number of rotors at Early Stabilization was 356). Percentage values for all regions sum up to 100% for each induction. Anatomical regions are according to the anatomy diagram in panel A of Figure S2. Comparisons were made by t-test for normal distributions (Shapiro-Wilk test) and by Wilcoxon signed-rank test for non-normal distributions. Statistical significance level is Alpha=0.025 for dual comparisons. See Supplemental Results section for more details.

Figure S7. Maximal dominant frequency (DFmax) in different atrial regions calculated at 4 different time periods following the S2 stimulus.
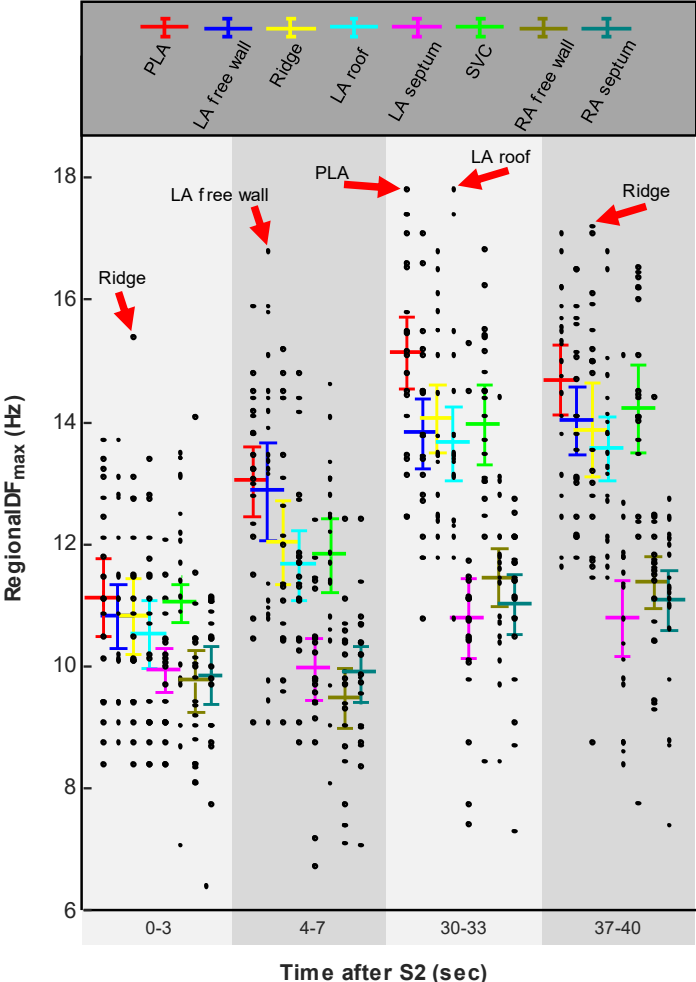

Colored symbols are mean±STD values for 20 AF inductions in 5 hearts for each region listed in the legend on top (20 dot symbols in each column correspond to 20 DFmax values at each particular location). Anatomical regions are according to the anatomy diagram in panel A of Figure S2. DFmax values at the PLA were compared with the DFmax values of regions with the nearest lower mean value by t-test.

Figure S8. Time-course of cycle lengths (CLs).
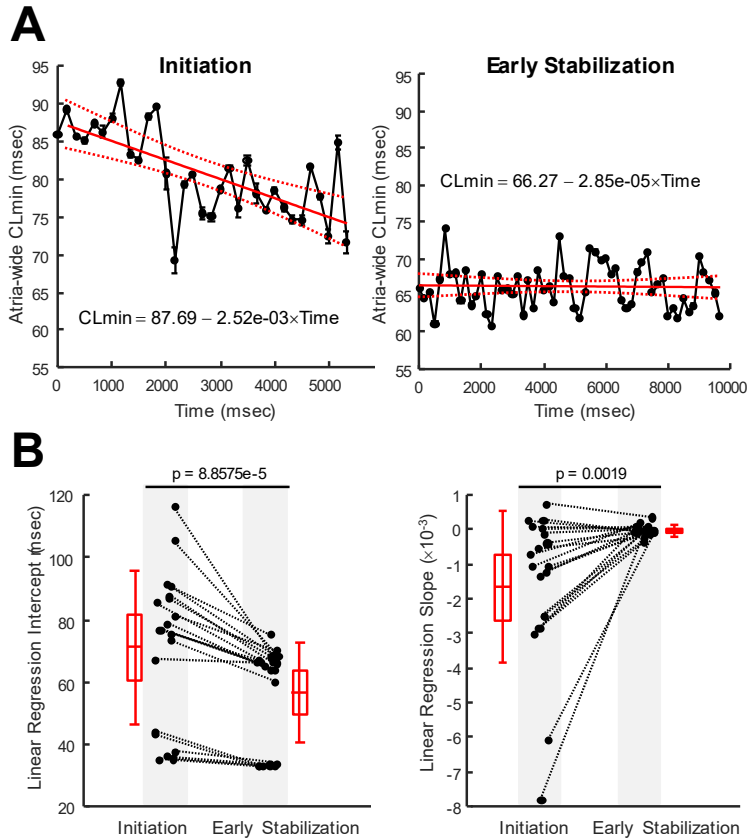
A) Representative induction example of minimal CL (CLmin) averaged over the mapped atria every consecutive 200 msec bin during Initiation (left) and Early Stabilization (right) stages of a sample AF induction. Linear best fit with 95% confidence lines are superimposed on graphs (red) and presented as formulas of with intercepts and slopes. **B)** Comparisons between Initiation and Early Stabilization stages for intercepts (left) and slopes (right) of CLmin time curses in AF inductions (N=5, n=20). Red markers indicate mean (horizontal bar), 95% confidence of the mean (box) and STD (error bars) values. Wilcoxon signed rank test was performed for all comparisons.

Figure S9. Appearance rate and time lifespan of rotors in each consecutive 1 sec long bins of time during Initiation and Early Stabilization of 20 AF inductions in 5 hearts.
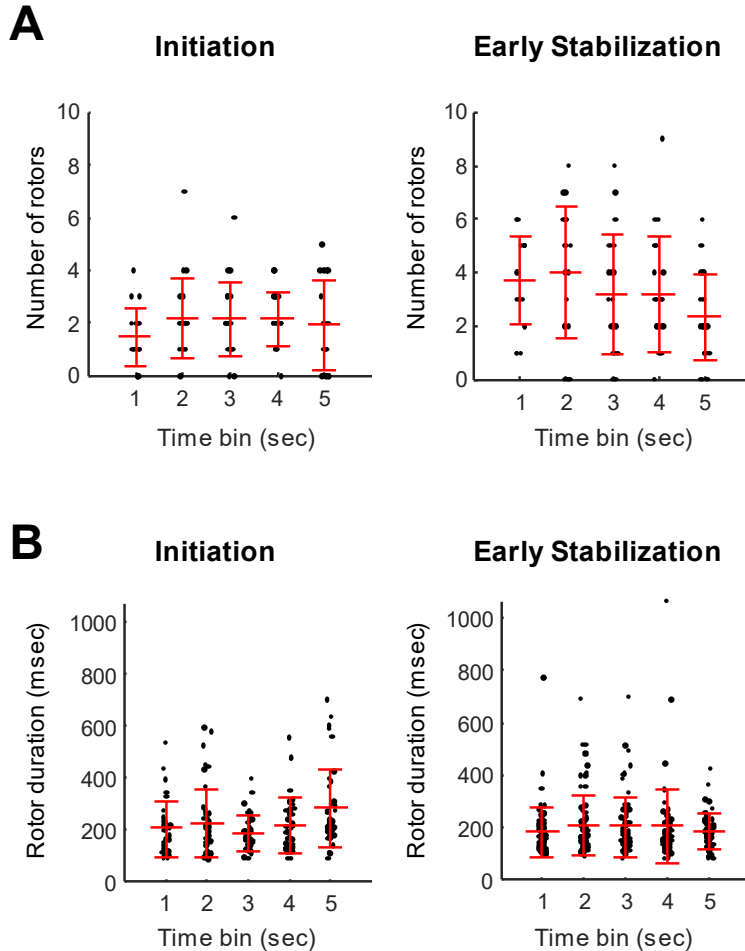

A total of 217 and 357 rotors during Initialization and Early Stabilization stages, respectively, were analyzed. **A)** Left: Numbers of rotors that appeared in each sequential 1 sec long bin during Initiation. Right: Left: Numbers of rotors that appeared in each sequential 1 sec long bin during Early Stabilization. There were no significant differences between inter-bin rates of appearance at the two stages (ANOVA tests. Initiation: p=0.4743, Early Stabilization: p=0.1253). Rotors appeared in the 20 AF inductions in series at 5 sec average rates of 2.0±1.37 vs. 3.29±2.09 rotors/sec during Initiation and Early Stabilization, respectively (p<0.0001). **B)** Left: Rotor durations for 217 rotors during Initiation. Right: Rotor durations for 357 rotors during Early Stabilization. ANOVA tests on inter-bin time lifespan of rotors revealed significant variability during Initiation (left, p=0.0062) and non-significant variability during Early Stabilization (right, p=0.5423). The 5 sec average time lifespan of the rotors decreased from 224.1±118.8 to 196.6±110.4 msec, respectively, (p=0.0074). Red symbols

are mean±STD values for 20 AF inductions (A), and for rotors (B), for each time bin in 5 hearts.

Figure S10. A sample case of decelerating LA CLs from before to after a rotor presence during the AF Initiation.
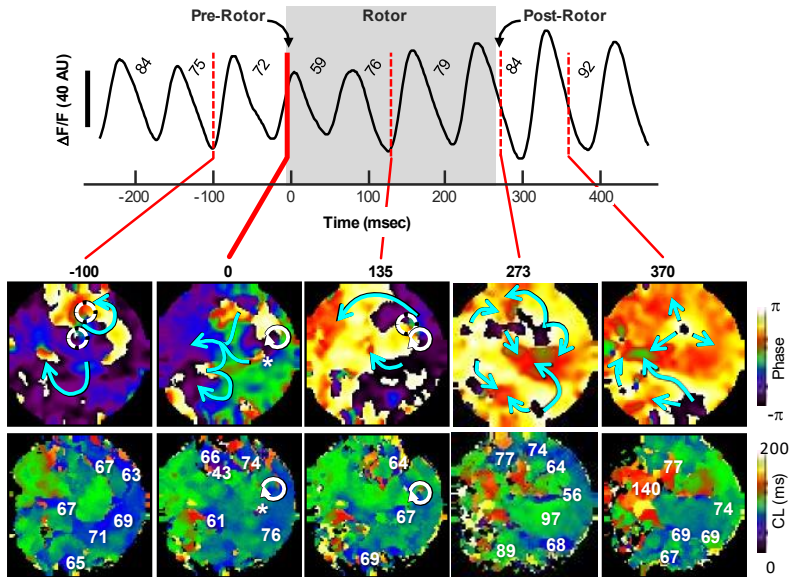
Fluorescence signal from a site near a rotor with corresponding phase (top row) and CL (bottom row) maps. Numbers superimposed on the fluorescence signal and in the CL maps indicate corresponding CLs in msec. Asterisks in maps indicate location of the fluorescence signal near the rotor. A stable rotor with undetected drift is present between 0 and 270 msec. The CLs in the sample fluorescence signal (top) prolong from tor values of 75 and 72 msec prior to the rotor formation to values of 84 and 92 msec after its disappearance. CL map after rotor disappearance (273 and 370 msec) is seen to have larger red-yellow areas and less blue areas compared with the CL map before rotor formation (0 and -100 msec) indicating a deceleration during the rotor presence. Pre-rotor and Post-rotor black arrow markers in the fluorescence trace indicate times of determining atria-wide CLmin in the analyses presented in Figures 4, S10 and S11. Arrowhead circles, sample rotor location and chirality. Arrows, general propagation directions. Dashed line circles, sample non-rotor SP locations.
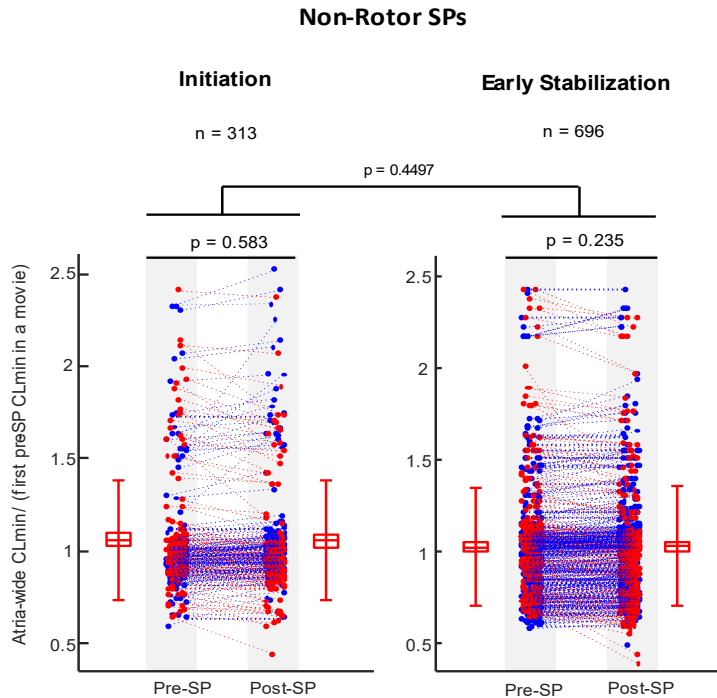
Figure S11. Analysis of rotors effect on atria-wide CLmin.
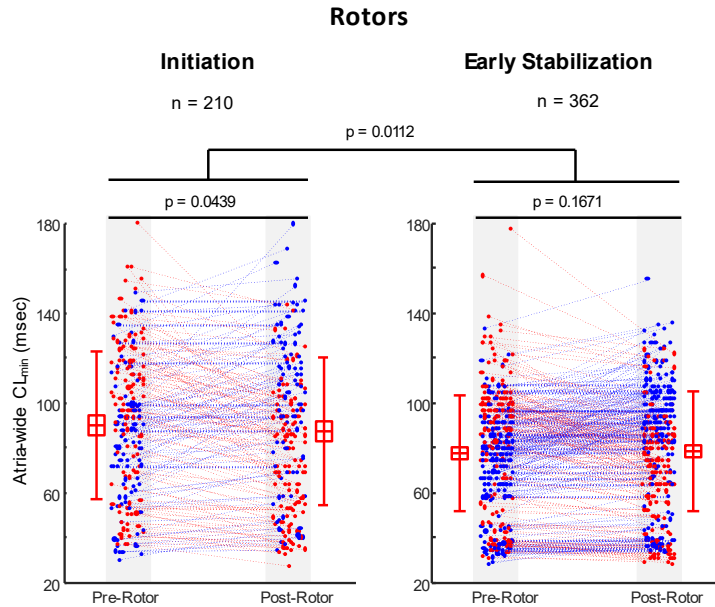
The CLmin values were determined from instantaneous panoramic CL maps pre- and post-rotors (regardless of their location) during Initiation (left) and Early Stabilization (right) of 20 induced AF episodes in 5 hearts. In each graph the CLmin pre- and post-rotors are paired and colored blue if post-rotor CLmin is larger than pre-rotor CLmin (deceleration), and in red if post-rotor CLmin is smaller than pre-rotor CLmin (acceleration). Red markers indicate mean (horizontal bar), 95% confidence of the mean (box) and STD (error bars) values. During Initiation (left, n=210), 113 (53.8%) pair cases demonstrated CLmin acceleration of (mean±STD) -20±18.9 msec and 97 pair cases demonstrated CLmin deceleration of 16.4±15.5 msec (Wilcoxon test p=3.81e-13). Cumulative analysis of all post- vs. pre-rotor CLmin during Initiation demonstrated a CLmin shortening from 90.2±32.3 msec to 87.3±33 msec (paired t-test p=0.0439). During Early Stabilization (right, n=362), 156 (43.1%) pair cases demonstrated CLmin acceleration of -15.2±13.7 msec and 206 pair cases

demonstrated CLmin deceleration of 14±13.9 msec (Wilcoxon test p=1.57e-22). A cumulative analysis of all post- vs. pre-rotor CLmin during Early Stabilization demonstrated a non-significant cumulative CLmin alteration from 77.6±26 msec to 78.7±26.9 msec (paired t-test p=0.1671).

Figure S12. Analysis of non-rotors (SPs with lifespan <1 rotation) effect on atria-wide CLmin.

CLmin values were determined from instantaneous panoramic CL maps pre- and post-SP (regardless of their location) during Initiation (left, n=313) and Early Stabilization (right, n=696) of 20 induced AF episodes. In each graph the CLmin pre- and post-SP are normalized to the first pre-SP CLmin in the corresponding Initiation or Early Stabilization movies, paired, and colored blue if post-SP CLmin is larger than pre-SP CLmin (deceleration), and in red if post-SP CLmin is smaller than pre-SP CLmin (acceleration). Among the 313 pairs Initiation pairs (left), 145 (46.3%) showed acceleration and 168 showed deceleration. Among the 696 Early Stabilization pairs (right), 278 (39.9%) showed acceleration and 418 showed deceleration. Red markers indicate mean (horizontal bar), 95% confidence of the mean (box) and STD (error bars) values. Cumulative analysis of post- vs. pre-SP CLmin in Initiation pairs (left) demonstrates non-significant alteration of normalized CLmin from 105.8±32.0% to 105.5±32.3% (mean±STD, paired t-test p=0.583). Similar analysis of Early Stabilization pairs (right) also demonstrates a non-significant normalized CLmin alteration from 102.8±32.0% to 102.9±32.4% (mean±STD, paired t-test p=0.235).

Supplemental Video Legends:

Video S1. Fluorescence movie of panoramic mapping of the endocardial RA and LA surfaces on the left and right sides of the frames, respectively. The movie shows waves crossing the LA and RA following the S1 pacing stimuli at the lateral aspect of the LA (right side of the movie). Movie is shown at a slowed frame rate. Best viewed with Windows Media Player.

Video S2. Fluorescence movie of panoramic mapping of the endocardial RA and LA surfaces on the left and right sides of the frames, respectively. The movie shows initially the tail of the last S1 wave in the RA, followed by a S2 wave and thereafter the initiation stage of AF. Movie is shown at a slowed frame rate. Best viewed with Windows Media Player.

Video S3. Fluorescence movie of panoramic mapping of the endocardial RA and LA surfaces on the left and right sides of the frames, respectively. Movie was recorded during the early stabilization stage of AF (about 30 sec following the S2 stimulus). Movie is shown at a slowed frame rate. Best viewed with Windows Media Player.

Video S4. Phase movie of panoramic mapping of AF initiation. The endocardial RA and LA surfaces are on the left and right sides of the frames, respectively. The movie shows initially the tail of the last S1 wave in the RA, followed by a S2 wave and thereafter the initiation stage of AF. Movie is shown at a slowed frame rate. Best viewed with Windows Media Player.

Video S5. Phase movie during the early stabilization stage of AF (about 30 sec following the S2 stimulus). The endocardial RA and LA surfaces are on the left and right sides of the frames, respectively. Movie is shown at a slowed frame rate. Best viewed with Windows Media Player.

Video S6. Phase movie of the LA at the Initiation stage showing a rotor drift as described in Figure 5. Movie is shown at a slowed frame rate. Best viewed with Windows Media Player.